DANMARKS OG GRØNLANDS GEOLOGISKE UNDERSØGELSE **RAPPORT 2021/39**

Response of the Paleocene sand reservoir and seal of the Nini Field to CO_2 – results of batch experiments

Project Greensand Phase 1 WP2

Hanne D. Holmslykke, Rikke Weibel, Hans Jørgen Lorentzen & Niels H. Schovsbo

GEOLOGICAL SURVEY OF DENMARK AND GREENLAND
DANISH MINISTRY OF CLIMATE, ENERGY AND UTILITIES

GEUS

DANMARKS OG GRØNLANDS GEOLOGISKE UNDERSØGELSE **RAPPORT 2021/39**

Response of the Paleocene sand reservoir and seal of the Nini Field to CO_2– results of batch experiments

Project Greensand Phase 1 WP2

Hanne D. Holmslykke, Rikke Weibel, Hans Jørgen Lorentzen & Niels H. Schovsbo

Released 01.10.2022

GEOLOGICAL SURVEY OF DENMARK AND GREENLAND
DANISH MINISTRY OF CLIMATE, ENERGY AND UTILITIES

G E U S

Response of the Paleocene sand reservoir and seal of the Nini Field to CO_2 – results of batch experiments

Project Greensand WP 2 phase 1

Hanne D. Holmslykke, Rikke Weibel, Hans Jørgen Lorentzen & Niels H. Schovsbo

Appendices:

Appendix 1: Raw data from the laboratory experiments (only as excel sheet)

Appendix 2 Results of BET analysis

Appendix 3: Chemical composition of the brine in the CO_2:brine:rock and the no CO_2:brine:rock systems. Compositions not corrected for extracted volume during sampling or back calculated to experimental conditions

Appendix 4: Heavy metal release

Appendix 5: Kinetic parameters applied for the geochemical modelling

Appendix 6: Results of the geochemical modelling

Abstract

Storage of CO_2 in the subsurface is one mean of effectively remove CO_2 from the atmosphere and reduce climatic changes. The Nini West Field, Danish Central Graben, represents a potential CO_2 storage site. A series of batch experiments have been conducted to investigate the hydrogeochemical reactions between CO_2, and the Paleocene sandstone reservoir of the Nini West Field, Danish Central Graben, and the overlying seal mudstone. Cleaned and uncleaned samples from the oil leg were investigated. To distinguish between the reactions caused by disequilibrium with the brine and those originating from CO_2 exposure, experiments with CO_2 saturated brine as well as brine without CO_2 were performed. Water samples were extracted continuously during the experiments to monitor the changes in the chemical composition of the brine after 4, 10, 14, 26, 46, 61 and 83 days of experimental run. Comprehensive post experimental back-calculations to experimental conditions were made to estimate the true chemical concentrations at experimental conditions.

Mineralogical changes during the experiments were identified by petrographic analysis of the rock material prior to and after termination of the experiments. Subsequently, geochemical models were made to help identify the chemical reactions between CO_2 and reservoir rock material and between CO_2 and the seal rock mudstone. The models were calibrated against the observed changes in the brine composition measured.

For both reservoir and seal, the most noticeable changes in the water chemistry are a decrease in the pH and an increase in the alkalinity and the aqueous concentrations of Fe^{2+}, Mn and Si.

For the reservoir, the results of the geochemical modelling show that the presence of CO_2 leads to:

- A significant increase in the initial dissolution of calcite followed by reprecipitation of calcite. The model does not predict calcite reprecipitation in the absence of CO_2. Calcite dissolution is not confirmed by the petrographic analysis, but is never the less crucial to fit the modelled concentrations of the components of the carbonate system (pH, alkalinity and Ca) to the measured values.
- An increase in the dissolution of Mn-bearing siderite followed by precipitation of a pure Fe-siderite. The model does not predict reprecipitation of siderite in the absence of CO_2. Alternatively, the relatively lower release of Fe to solution compared to Mn could potentially result from dissolution of a siderite with a different chemical composition or reprecipitation of ironhydroxides.
- Dissolution of an Fe-containing mineral. In the model berthierine has been applied.
- Mass balance considerations of the CO_2 and reservoir system indicate that only small fractions of the reservoir rock react during the experiment. Thus, the composition of the sandstone after the experiments calculated by mass balance considerations of the results of the geochemical model equals that determined by point counting prior to the experiment.

The presence of hydrocarbons does not seem to affect the nature of the dissolution/precipitation processes between the Paleocene sandstone reservoir of the Nini West Field and CO_2. The presence of hydrocarbons may affect the reaction rates; however, it is uncertain if this is due to heterogeneities or that the hydrocarbons block some of the reactive sites on the minerals.

The results of the geochemical model indicate that for the seal, the presence of CO_2 may lead to:

- Increased dissolution of calcite and siderite.
- Dissolution of an Fe-bearing mineral. The identification of this mineral is uncertain. In the model illite was used.
- It is unclear whether heulandite dissolves or precipitates in the presence of CO_2 the petrographic analysis contradicts the model.
- Based on mass balances it is estimated only an insignificant fraction of the seal mudstone has reacted during the experiment. Thus, the composition of the seral mudstone after the experiments calculated by mass balance considerations of the results of the geochemical model equals that determined by point counting prior to the experiment.

The results of this study suggest that only minor constituents of the reservoir and seal rock material is reactive towards CO_2. In both the reservoir and seal experiments reactions associated with the initial brine chemical composition and the rock matrix were observed suggesting that the starting brine composition estimated from the produced water should be altered in future experiments. We suggest using the chemical composition measured at the end of the experiments i.e., at day 83 without CO_2 as a starting point in new experiments in order to be as close to equilibrium conditions in the reservoir and seal.

1. Introduction

This report summarises the results of the compatibility analysis of the Paleocene sandstone reservoir of the Nini West Field to CO_2 conducted within the “Project Greensand” funded by EUDP. The main objective of the Project Greensand is to investigate if the Paleocene sandstone reservoir of the Nini West Field in the Danish North Sea can be used for safe long-term storage of CO_2. The purpose of these compatibility analysis, made as “batch experiments”, is to investigate if core material from the Nini reservoir and its seal is compatible with storage of supercritical CO_2. During storage of supercritical CO_2, the formation water is likely to become gradually saturated with CO_2. Since CO_2 saturated formation water is more aggressive/corrosive towards reservoir sandstone and overlying seal, the batch experiments were conducted with CO_2 saturated formation water. Previous experiments tested the reservoir for one month only and served as test cases for longer batch experiments (Holmslykke et al. 2021). The main focus of this report are the results of the subsequent batch experiments performed with the aim of identifying potential geochemical reaction between the Paleocene sandstone reservoir of the Nini West Field and the overlying cap rock material and CO_2.

Acknowledgment
The Danish Energy Technology Development and Demonstration Program (EUDP) is greatly acknowledged for its funding of the “Project Greensand”. The Project Greensand is carried out by INEOS, Maersk Drilling and Wintershall DEA and the lead author thanks the team for valuable comments and suggestions that improved the content of this report.

2. Materials and methods

2.1 Sample description and preparation

In total 14 1.5" core samples from the Nini-4 well were selected for the geochemical batch experiments (Table 2.1). Two of these core samples were used in the preliminary batch experiments and the results of these are reported in Holmslykke et al., (2021). The remaining core samples were divided in two and used for two identical set of experiment: one set with the aim of calibrating the geochemical model and the other set running for slightly longer time with the aim of validating the geochemical model. In this report focus is on the calibration of the hydrogeochemical model, however, all data are presented in Appendix 1.

For each of the two set of batch experiments, consisting each of six core samples, four of the core samples were selected from the Paleocene sandstone reservoir and the other two from the overlying seal. The samples from the reservoir were prepared and had porosity and permeability analysed by Robertson Research Institute (RRI). Two of the reservoir samples were cleaned and did not contain oil, whereas the other two were preserved samples and as such contained oil. The latter two samples were cleaned slightly with toluene to remove some of the oil so that the samples represent the present day situation where the major part of the hydrocarbon has been extracted. The two samples from the seal were prepared by GEUS as part of this project. They were not cleaned by prior to analysis but prepared "as is".

Table 2.1 Overview of plug specimens selected for the geochemical batch experiments.

Sample ID	Experiment	Formation	Condition	Depth (ft)	
111	1 month, CO_2	Reservoir	Oil-free	1781.66	[1)]
113	1 month, N_2	Reservoir	Oil-free	1782.3	[1)]
98	Res., N_2	Reservoir	Oil-free	1777.32	Calibration
104	Res., CO_2	Reservoir	Oil-free	1779.32	
98B	Res., HC, N_2	Reservoir	Oil-containing	1777.22	
104B	Res., HC, CO_2	Reservoir	Oil-containing	1779.27	
15	Seal, N_2	Seal	As is	1748.65	
15C	Seal, CO_2	Seal	As is	1748.70	
92	Res., N_2	Reservoir	Oil-free	1775.33	Validation
95	Res., CO_2	Reservoir	Oil-free	1776.32	
92B	Res., HC, N_2	Reservoir	Oil-containing	1775.27	
95A	Res., HC, CO_2	Reservoir	Oil-containing	1776.27	
13C	Seal, N_2	Seal	As is	1762.15	
13B	Seal, CO_2	Seal	As is	1762.27	

[1)]Reported by Holmslykke et al. (2021)

Prior to the experiment, a slice of approximately 0.5 cm thickness was cut from the plug specimens and divided into either two or four pieces. One of these pieces were selected and used for petrographic analysis to determine the mineralogy of the plug specimen prior to the experiment. The remaining pieces were used in the experiment and used for petrographic analysis of the tested material after the experiment. The remaining larger part of the reservoir specimens were crumpled by hand to avoid breaking the glauconite grains, while the seal samples were crushed to a diameter of 250 µm to enhance chemical reactions by exposing large amounts of the sample to the fluid.

2.2 Fluid composition

The chemical composition of the synthetic Nini formation water used in the batch experiments represents the P50 composition of produced water from the Nini field (c.f. Olsen et al. 2020, Holmslykke et al. 2021). The saturation state of the produced water was tested using PHREEQC v3 (Parkhurst and Appelo, 2013) and the formation water composition modified accordingly. For example, the model indicates that the measured produced water is super saturated with respect to calcite. However, due to the high reactivity of calcite, it is highly unlikely that the formation water is super saturated with respect to calcite. Thus, the modelled super saturation of the produced water most likely reflects uncertainties in the measurements and therefore the concentration of HCO_3^- is adjusted to a level where the formation water is in equilibrium with calcite. In a similar manner, the concentration of Ba is adjusted to satisfy equilibrium considerations with respect to barite.

Preliminary experiments where samples of the Paleocene sandstone reservoir from the Nini-4 well reacted with synthetic Nini formation water with and without CO_2, showed that even in the absence of CO_2, dissolution of siderite occurred (Holmslykke et al., 2021). For practical reasons, iron was not added to the synthetic formation water in these experiments. To minimise the dissolution of siderite due to disequilibrium of the synthetic formation water in the batch experiments of this study, Fe^{2+} was added in a concentration corresponding to equilibrium with siderite at ambient temperatures as calculated with PHREEQC and its Pitzer database. Iron was added via an Fe^{2+} stock solution (0.8M Fe^{2+}) and all work related to the addition of Fe^{2+} to the synthetic formation water was made in an anaerobic glovebox.

The measured concentration of the Nini synthetic formation water used for the batch experiments are given in Table 2.2.

Table 2.2 Measured composition of the synthetic Nini formation water used in the batch experiments.

Element		Concentration
Na	mmol/L	1255
K	mmol/L	5.4
Mg	mmol/L	40
Ca	mmol/L	119
Sr	mmol/L	0
Ba	mmol/L	0
Fe	mmol/L	0.13
Cl	mmol/L	1607
SO_4^{2-}	mmol/L	0.19
Alkalinity	meqv/L	0.18

2.3 Experimental procedure

2.3.1 Batch assemblage and experimental rig

All batch cylinders were assembled inside an anaerobic glovebox to avoid intrusion of atmospheric oxygen into the batch cylinders, and oxidation of the Fe^{2+}-containing synthetic brine. All materials and equipment used for addition of Fe^{2+} to the brine and assemblage of the batch cylinders were stored inside the glovebox overnight. Before loading the batch cylinders into the glovebox, *c.* 100 mL distilled water was added to each cylinder on the back side of the piston (cf. Figure 3.1) to enable the piston to retract during the subsequent heating of the brine, addition of CO_2, etc. As preparation for addition of Fe^{2+} to the synthetic brine, a synthetic brine without Fe was made outside the glovebox and degassed before being stored inside the glovebox overnight. Additionally, a bottle of distilled water was degassed and purged with N_2 that had passed through a Cu-column to remove any traces of oxygen in the N_2. This distilled water was used to make an Fe- standard solution together with newly bought $FeCl_2$-powder.

Upon assemblage, 75 g of core material (Table 2.1) was transferred to a ProLight Ti-690-64-FF piston cylinder. Depending on the experiment (Table 2.3), a calculated amount of Fe-containing brine was added to the piston cylinder before the cylinder was tightly closed. A smaller volume of brine was added to the experiments with CO_2 saturated brine to account for the following addition of CO_2. After the subsequent addition of CO_2 all batch experiments initially had a water:rock ratio of 6.

Table 2.3 Overview of masses of core material, brine and CO_2 in the all the batch experiments.

Sample ID	Experiment	Mass crum-bled ma-terial	Mass 1/4 slice	Mass 1/4 slice	Mass 1/2 slice	Total mass of solid	Mass brine	Vol. CO_2	Mass CO_2	
		g	g	g	g	g	g	ml	g	
111	1 month, CO_2									*
113	1 month, N_2									*
98	Res., N_2	67.98	3.65	3.23		74.86	459			Calibration
104	Res., CO_2	68.33	4.04	2.54		74.91	442	22.33	16.12	Calibration
98B	Res., HC, N_2	62.46			12.55	75.01	460			Calibration
104B	Res., HC, CO_2	62.09			12.91	75.00	442	22.33	16.12	Calibration
15	Seal, N_2	69.01			5.99	75.00	468			Calibration
15C	Seal, CO_2	70.61			4.39	75.00	442	22.33	16.12	Calibration
92	Res., N_2	62.45			9.43	75.00	460			Validation
95	Res., CO_2	60.98			10.56	74.99	443	22.33	16.12	Validation
92B	Res., HC, N_2	60.31			14.70	75.01	460			Validation
95A	Res., HC, CO_2	63.63			11.35	75.00	443	22.33	16.12	Validation
13C	Seal, N_2	68.85			6.16	75.01	460			Validation
13B	Seal, CO_2	69.25			5.74	75	433	22.33	16.12	Validation

* Reported by Holmslykke et al. (2021).

Once securely tightened, the batch cylinders were removed from the glovebox and connected one by one to a Vindum pump. Any free gas phase in the batch cylinders were removed by placing the cylinder in a vertical position and slowly injecting distilled water on the back side of the piston until brine became visible at the valve on the top of the cylinder. Following this procedure, the batch cylinders were transferred to an oven with a temperature of 60°C (Figure 2.1). The pressure of the batch cylinders was increased overnight to 199 bara using a Vindum pump. Once a stable pressure of 199 bara and temperature of 60°C were reached, CO_2 was added to the batch cylinders for the experiments with CO_2 (cf. section 2.3.2).

During the experiment, the batch cylinders were placed in a cradle-like device allowing the batch cylinders to tip back and forward. Mixing of the fluid inside the batch cylinders were ensured by manually tipping the batch cylinders back and forward at least once a day. During sampling of the batch cylinders (cf. section 2.3.3) the brine end of the cylinders were always in the top position so that the core material was in the lower part of the cylinder, thereby minimising the risk of extraction of core material while sampling brine.

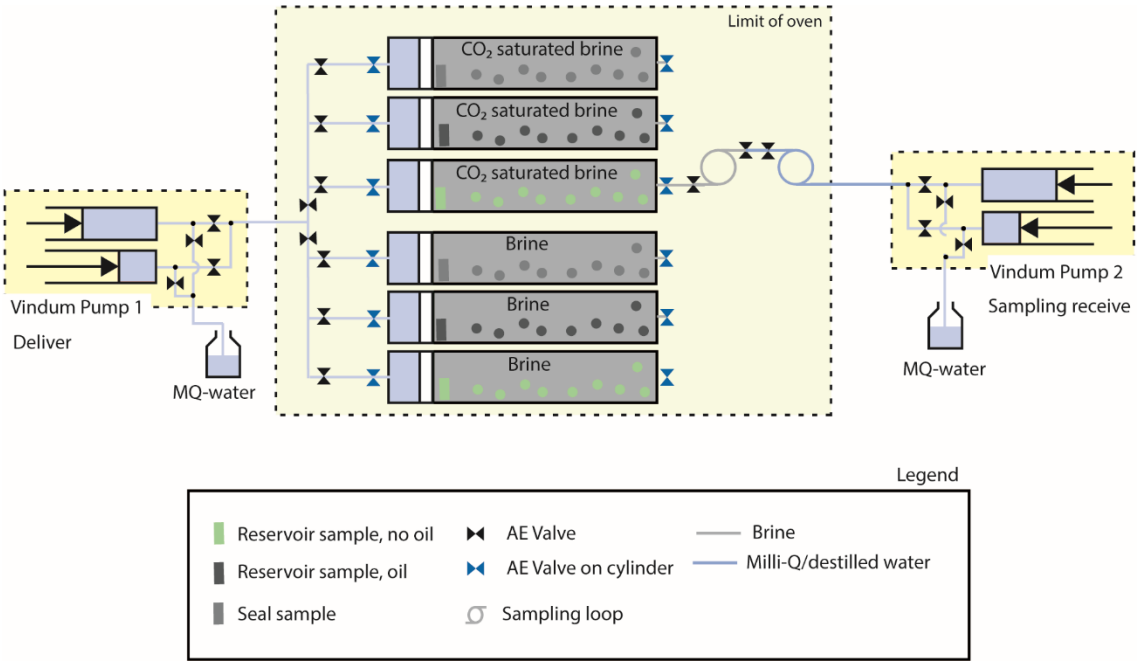

Figure 2.1 *Schematic illustration of the experimental set up for the batch experiments.*

2.3.2 Procedure for saturation of brine with CO_2

For the experiments with CO_2, CO_2 saturated formation brine was prepared by first transferring 442 g freshly prepared and degassed brine (Table 2.2) into a ProLight Ti-690-64-FF piston cylinder as described in section 2.3.1. After increasing the pressure to 199 bara and temperature to 60°C, the sample cylinder with formation brine was connected to another sample cylinder containing CO_2 (Anaerobe carbon dioxide 4.0 diptube), also at 199 bara and 60°C. Following this, 22.3 mL CO_2 was transferred to the sample cylinder containing formation brine at a rate of 10 mL/h and the CO_2/formation brine mixture was left for at least 20 h. Complete dissolution of the CO_2 in the formation brine was assumed when the volume change in the CO_2/formation brine sample cylinder after the equilibration period of 20 h was less than ± 0.01 mL/h.

The amount of CO_2 required for saturation of the formation brine (8.62 wt% salinity) with CO_2 at 199 bara and 60°C was calculated using the EOS of Chang et al. (1998). However, in order to be confident that all CO_2 was dissolved in the formation brine and no separate CO_2 phase was present at any time in the experiment e.g., due to uncertainties in the calculations or minor pressure changes in the experiment, a CO_2 addition corresponding to 95% of saturation was used in the calculations. For the calculations, the density of aqueous NaCl solutions was found in Rowe and Chou (1970) while the thermodynamic data of NIST Standard Reference Database Number 69 were used for the CO_2.

2.3.3 Procedure for water sampling and chemical analysis

Water samples for chemical analysis were extracted after 4 d, 10 d, 14 d, 26 d, 46 d, 61 d and 83 d. A water sampling procedure was developed to allow extraction of representative water samples at reservoir conditions and, for the experiments with CO_2, to avoid uncontrolled degassing of CO_2 during the sampling procedure.

Prior to sampling, a primary sampling loop (18 mL) containing distilled water was connected to the batch cylinder from which a water sample was to be withdrawn (Figure 2.1). The primary sampling loop was connected to a secondary sampling loop, also containing distilled water, that was connected to a Vindum pump. The purpose of the secondary sampling loop was to ensure that formation brine did not enter the pump (Vindum pump 2 in Figure 2.1) during sampling. All valves on the sampling loops were open to ensure transfer of distilled water in the loops whereas the valve on the formation brine side of the cylinder was closed to ensure that no distilled water entered the batch cylinder (Figure 2.1). Once all the sampling loops were connected the pressure of the sampling loops was increased to 199 bara using Pump 2, so that the same pressure was applied in both the batch cylinder and the sampling loops. All valves on the distilled water side of the batch cylinders were closed except those allowing flow from the Vindum Pump 1 to the batch cylinder from which a water sample was to be withdrawn. Water sampling was initiated by opening the valve on the cylinder on the formation brine side of the batch cylinder and allowing pump 2 to receive water while pump 1 delivered water, both pumps with a rate of 100 mL/h. This allowed formation brine to be transferred from the batch cylinder to the sampling loop. At each sampling *c.* 22 mL was transferred to the primary sampling loop to ensure that all distilled water initially present in the primary sampling loop was replaced with formation brine. After the transfer of the formation brine, all valves were closed and the primary loop, now containing the water sample to be analysed, were removed from the oven and samples for chemical analyses extracted as soon as possible (within 1 – 2 minutes) to prevent precipitation of minerals inside the sampling loop due to the temperature decrease.

Samples for chemical analysis from the experiments without CO_2, were taken by immediately transferring the sample from the primary sampling loop to a syringe at ambient temperature and pressure. The pH was measured immediately on unfiltered samples using a Mettler-Toledo InLab® Micro pro pH electrode, freshly calibrated against dilute standard pH buffers. The remaining of the sample was filtered and analysed for major cations, anions, alkalinity and heavy metals.

For the experiments with CO_2, the water sample obtained at reservoir conditions in the primary sampling loop was immediately transferred to a sample cylinder with a larger volume placed outside the oven (Figure 2.2). Prior to the transfer, the sample cylinder was evacuated with a vacuum pump to ensure that any headspace pressure measured in the sample cylinder was caused by degassing (mainly of CO_2) from the water sample.

As part of the procedure where the formation brine at high pressure in the primary sampling loop is transferred to the secondary sampling loop with larger volume and lower pressure, CO_2 inevitably degasses from the water sample and a separate gas phase will form.

Equilibrium between degassed CO_2 and the water phase was assumed when a constant pressure was observed in the sample cylinder and the pH and pressure were measured. The pH of the cooled (to ambient temperature) sample was measured using a PRO140J-5M-BNC electrode connected to MeterLab pHM210 pH-meter and a Druck transducer was used for the pressure measurements. Subsequently, a gas sample was withdrawn and transferred to an exetainer under water to minimize the risk of contamination by atmospheric oxygen during the transfer as illustrated in Figure 2.3. Finally, a water sample was collected, filtered, and analysed for major cations, anions, alkalinity and heavy metals.

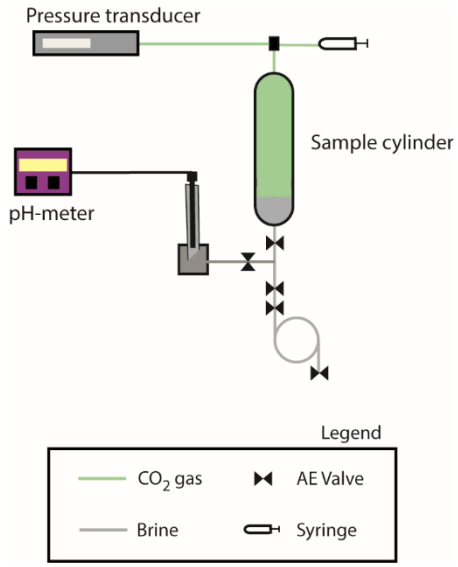

Figure 2.2 *Schematic illustration of the set up for pH measurement for the water samples from the experiments with CO_2.*

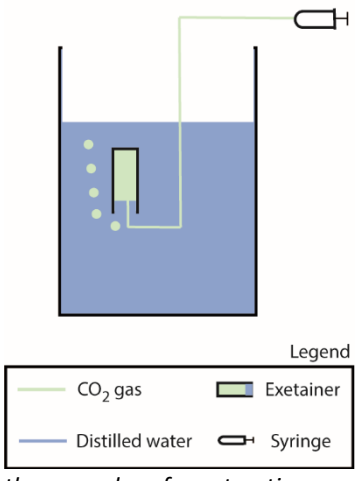

Figure 2.3 *Schematic illustration for the procedure for extracting gas analysis*

The water samples for chemical analysis were filtered through 0.2 µm Satorius cellulose acetate (CA) filters. The content of aqueous Fe^{2+} and total Fe was measured immediately after filtration and the alkalinity was measured immediately after the Fe measurements. Samples for analysis for cations and heavy metals received 0.4 vol% of 7M HNO_3, and were kept refrigerated until analysis while samples for anion analysis (Cl and SO_4^{2-}) were kept refrigerated until analysis.

Fe^{2+} and total Fe measurements were made using by the ferrozine method (Stookey, 1970). Alkalinity was determined by Gran titration (Appelo and Postma, 2005) of 2 mL aliquots with 0.001 M HCl for the samples from the experiments without CO_2 and 0.1 M HCl for the samples from experiments with CO_2. Major cations (Na, K, Ca and Mg) were measured by ion-chromatography (Metrohm IC, 819 detector, column C4-250-250/4.0) with a quantification limit of 0.05 mg/L. Heavy metals were measured by ICP-MS (PerkinElmer Elan 6100DRC, Elan software version 3.3) with a detection limit of 0.001-5 mg/L depending on the element. Samples for anion analysis (chloride and sulphate) were analysed by ion-chromatography (Metrohm IC, 819 detector, column Metrosep A sup. 5 – 150/4.0) with a quantification limit of 0.05 mg/L. To minimize matrix effects during analysis, all standards were prepared with the same matrix as the diluted fluid samples.

During the de-pressuring of the water sample in the sample cylinder, there is a risk that calcite precipitates due to the degassing of the CO_2. Therefore, after the water samples were withdrawn from the sample cylinder, the sample cylinder was rinsed in 5 mL 0.1% HNO_3 to dissolve any calcite that might have precipitated in the sample cylinder. The rinsing acid was subsequently analysed for major cations. No indications were, however, observed for precipitation of calcite in the sampling cylinder or visually in the bottom end of the pH housing.

2.3.4 Procedure for termination of the batch experiments

The batch experiments were terminated after 83 d. Immediately before termination of the experiments, the last samples for chemical analysis were extracted and prepared for analysis. Subsequently, the pressure was decreased in the batch cylinders by allowing pump 1 in Figure 2.1 to receive water with a constant rate of 25 mL/h while allowing the temperature to decrease overnight. The following day when ambient temperature and pressure was reached, each batch cylinder was carefully opened, and the rock material filtered through a 0.4 µm filter while cleaning the crumbled/crushed samples with methanol to remove any salt precipitations. Following this procedure, rock samples were separated for further cleaning with methanol to ensure sufficient cleaning. Subsequently, the samples were dried and prepared for further analysis. Petrographic analysis and specific surface area determination using Brunauer–Emmett–Teller method (BET analysis, Coulter SA 3100) of the core material were made prior to and after the experiments. Results of the analysis are presented in Appendix 2.

2.3.5 Procedures for post experimental corrections of measurements

2.3.5.1 Correction for extracted volume during sampling

During sampling, brine is extracted from the batch cylinder while core material remains in the batch cylinder. To account for this change in the water:rock ratio during the experiment, the measured chemical concentrations are corrected by assuming conservation of mass, as illustrated in Figure 2.4.

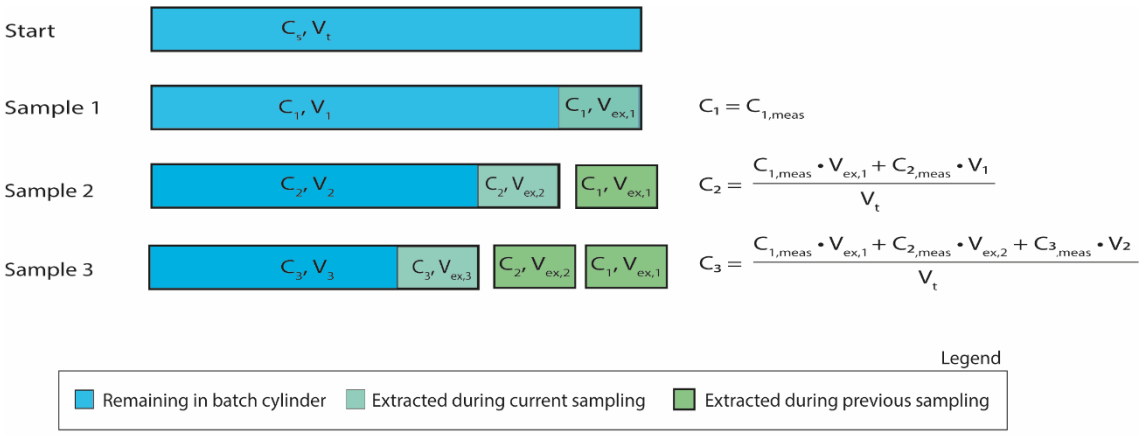

Figure 2.4 *Schematic illustration for the procedure for extracting gas analysis*

For example, the number of moles of a given aqueous specie at the time of sample 2 is the measured concentration ($C_{2,meas}$) times the volume of brine in the cylinder prior to extraction of sample 2 (V_1) plus the number of moles extracted in sample 1 ($C_{1,meas} \cdot V_{ex,1}$). The concentration at the time of extraction of sample 2 is then obtained by dividing the number of moles with the volume of brine present in the batch cylinder at the start of the experiment (V_t).

2.3.5.2 Concept for back-calculation to experimental conditions

Since all analytical measurements for the gas and water samples are made at ambient conditions back-calculations to experimental conditions is necessary. The experimental condition concentrations may be estimated by “back calculating” the measured chemical composition of the water samples to the applied reservoir pressure and temperature. Thus, numerical hydrogeochemical calculations were carried out using PHREEQC v3 (Parkhurst and Appelo, 2013).

For the experiments without CO_2 back-calculations are necessary mainly due to the temperature drop associated with the sampling procedure which causes an increase in the pH compared to the true reservoir condition pH. For these experiments, back-calculation to

experimental conditions is simply made using all measured data at each sampling time to make a speciation calculation at experimental pressure and temperature.

Additionally, for the experiments with CO_2, a controlled degassing of CO_2 from the water samples takes place during the sampling step where the water sample is transferred from the primary sampling loop at reservoir conditions to the secondary sampling cylinder. This causes an increase in the pH as compared to the true reservoir condition pH. Furthermore, the degassing of CO_2 drives the following chemical reaction towards the left:

$$CO_{2(aq)} + CaCO_3 + H_2O \leftrightarrow Ca^{2+} + 2HCO_3^- \quad (2.1)$$

Thus, there is a risk that some calcite may precipitate during the sampling procedure, and thereby that the Ca concentration decreases compared to the true reservoir condition Ca concentration. As mentioned in section 2.3.3 no indications were, however, observed for precipitation of calcite in the sampling cylinder or visually in the bottom end of the pH housing.
In order to estimate the true experimental condition chemical concentrations at the operation conditions of the experiments with CO_2, the chemical concentrations are calculated at three stages of the experiment: 1) at the operating conditions, 2) at the conditions measured in the secondary sampling cylinder 3) at the conditions of the water sample analysis. Particularly the pH, alkalinity and Ca-concentration are of interest in order to check consistency of the CO_2 sensitive chemical data. The calculations are carried out as a batch-like forward model of the experiments and the concept is illustrated in Figure 2.5 The following input and assumptions apply for each stage:

1) The input for the experimental conditions calculations is the known chemical composition of the formation brine, together with the expected chemical reactions during the experiments. Temperature and pressure are as applied in the experiment.

2) The input for the sampling point calculations is the chemical composition calculated at stage 2 combined with the sampling temperature and measured CO_2 pressure.

3) The input for the analysis point calculations equals those for stage two together with equilibrium with calcite. The assumption is that calcite has precipitated prior to the chemical analysis of the water sample.

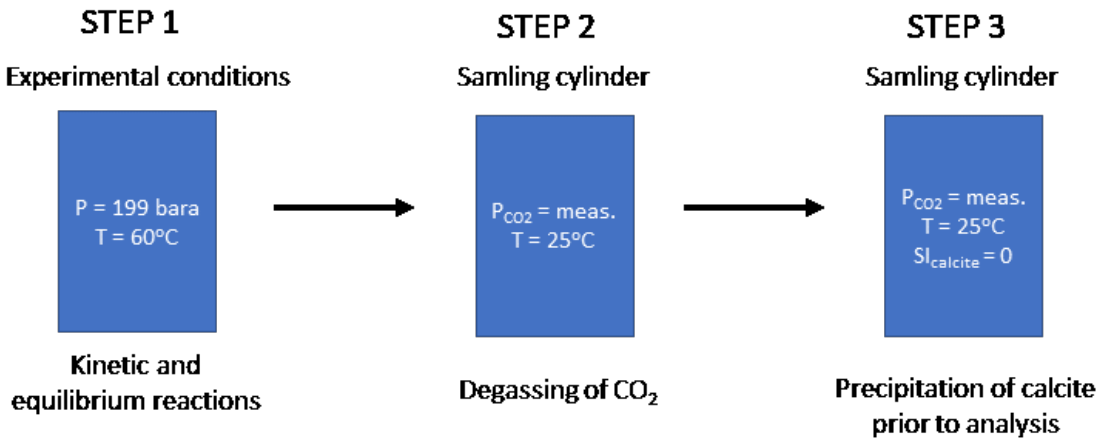

Figure 2.5 *Concept for estimation of experimental condition chemical concentrations of CO_2 sensitive chemical parameters. P_{Co2} denotes the CO_2 pressure and $SI_{calcite}$ denotes the saturation index with respect to calcite (SI = 0 corresponds to saturation).*

2.4 Post experimental procedures

2.4.1 Mineralogical analysis

For each batch experiment, two subsamples of the experimental plug were investigated in order to cover possible mineralogical changes in the core material during the experiment; a trim taken prior to the experiment and a trim exposed in the experiment. The sandstone trims were impregnated with blue epoxy, for easy identification of porosity, and prepared as polished thin sections prior to transmitted and reflected light microscopy. Supplementary studies of dissolution features were performed on carbon-coated thin sections and platinum-coated rock chips using a Zeiss Sigma 300 VP operating at 10–15 kV equipped with double Bruker energy dispersive X-ray spectrometers (EDS) with 30 mm^2 active areas. Modal composition of the sandstone was obtained by point counting 500 points of the mineral phases, in addition to the porosity.

Mineralogical composition of the mudstone seal samples was obtained by X-ray diffraction (XRD) of bulk rock samples and clay fraction performed at DTU. Samples for bulk rock analysis were crushed in a wolfram-carbide mortar to a size faction < 45 µm. The powder was pressed into a disk prior to bulk rock analysis. Clay samples were prepared by suspending 0.03 g of the clay fraction into 1.5 mL distilled water and spread evenly over a glass plate and dried 24 hours. Subsequently, the samples were saturated with ethylene glycol for two days at 60°C, before analysis. For heat treatment, samples were first heated to 350°C in an oven for 2 hours and left to cool overnight, before analysis. Second heat treatment was at 550°C. Both randomly oriented bulk samples and oriented clay fraction samples were analysed by a Panalytical-X-Pert Pro. Semi-quantification was performed by multiplying peak height with correction factors similar to the method by Hillier (2003).

Two bulk rock samples were scanned on a Bruker-AXS diffractometer D8 Advance with primary beam Ge111 monochromated CuKα radiation and a LynxEye silicon-strip detector at Copenhagen University. Quantification of major mineral phases was done by Rietveld analysis of X-ray diffractograms of bulk-rock samples. The results were used to adjust the correction factor of heulandite.

2.4.2 Numerical analysis

The compatibility of the reservoir and seal material respectively with CO_2 was modelled using the numerical software PHREEQC version 3.0 and its database phreeqc.dat (Parkhurst and Appelo, 2013). Combined with the petrographic analysis, the hydrogeochemical modelling helps identify which minerals may possibly dissolve and/or precipitate during the experiments. To mimic the experimental set up, a batch-like forward model of the experiments were made. Input for the model is the chemical composition of the Nini formation water (Table 2.2), the amount of CO_2 added to the experiment (Table 3.1) and identified mineralogical changes during the experiments. Chemical reactions were allowed for 83 days at 60°C and 199 bara.

The model includes the thermo-kinetic processes of mineral dissolution/precipitation reaction using the kinetic rate law given by (Palandri and Kharaka, 2004; Appelo and Postma, 2005):

$$r = k \cdot \frac{A_0}{V} \cdot \left(\frac{m}{m_0}\right)^{0.67} \cdot (1 - \Theta) \tag{2.2}$$

where r is the dissolution/precipitation rate (mol/L/sec), k the overall rate constant (mol/m^2/sec), A_0 the initial surface area (m^2), V the liquid volume (L), m the remaining mass of mineral, m_o the initial mass and θ the mineral saturation ratio given by $\theta = IAP/K$, where IAP is the ionic activity product and K the equilibrium constant. The term $(m/m_0)^{0.67}$ corrects for changes in reactive surface sites during the dissolution/precipitation process (Appelo and Postma, 2005).
The rate constant k as function of temperature is calculated by the Arrhenius equation:

$$k = k_{25} exp\left[\frac{-E_a}{R}\left(\frac{1}{T} - \frac{1}{298.15}\right)\right] \tag{2.3}$$

where E_a is the activation energy (J/mol), k_{25} the rate constant at 25°C, R the gas constant (J/mol/K) and T the temperature (K). In addition to dissolution in pure water (neutral mechanism), the dissolution and precipitation of alumino-silicates may be controlled by H^+ (acid mechanism) and OH^- (alkaline mechanism). The overall rate constant is thus given by (Palandri and Kharaka, 2004):

$$k = k_{25}^{N} exp\left[\frac{-Ea^{N}}{R}\left(\frac{1}{T} - \frac{1}{298.15}\right)\right] + k_{25}^{A} exp\left[\frac{-Ea^{A}}{R}\left(\frac{1}{T} - \frac{1}{298.15}\right)\right] a_H^{n_A} + k_{25}^{B} exp\left[\frac{-Ea^{B}}{R}\left(\frac{1}{T} - \frac{1}{298.15}\right)\right] a_H^{n_B} \tag{2.4}$$

where the indices *N*, *A* and *B* refer to neutral, acid and alkaline mechanisms, respectively and *a* represents the activity of the species.
For carbonates the dissolution/precipitation mechanisms depend on HCO_3^- and reaction rates depend on the CO_2 pressure (P_{CO2}) (Carbonate mechanism). The overall rate expression for carbonates is therefore:

$$k = k_{25}^{N} exp\left[\frac{-Ea^{N}}{R}\left(\frac{1}{T} - \frac{1}{298.15}\right)\right] + k_{25}^{A} exp\left[\frac{-Ea^{A}}{R}\left(\frac{1}{T} - \frac{1}{298.15}\right)\right] a_{H}^{n_A} + k_{25}^{C} exp\left[\frac{-Ea^{C}}{R}\left(\frac{1}{T} - \frac{1}{298.15}\right)\right] P_{CO2}^{n_B} \quad (2.5)$$

where the indices *C* refer to the carbonate mechanism.

The rate of heulandite dissolution is found by Ragnarsdottir (1993).

The same kinetic expression is assumed for both dissolution and precipitation processes (Cantucci et al., 2009). The initial amount of the minerals (m_0) was estimated by point counting of thin sections (cf. section 3.1.2) while rate constants and the initial specific surface area of the minerals were found in the literature (André et al., 2007; Cantucci et al., 2009).

The models were fitted to the observed changes in the chemical composition of the brine by adjusting to the specific surface area. A reasonable fit of the model output to the experimental data indicates that the model mimics the reactions occurring the experiments.

3. Results and discussion

3.1 Reservoir

3.1.1 Measured changes in brine composition

Post experimental corrected changes in the brine composition due to chemical reactions between the Paleocene sandstone reservoir material (cleaned and with hydrocarbons) of the Nini West Field and brine saturated with CO_2 and in the absence of CO_2 is shown in Figure 3.1. Uncorrected data for all experiments are listed in Appendix 1 and illustrated Appendix 3. In all measurements, the concentration of aqueous Fe^{2+} equals that of total aqueous Fe. Significant increases are observed for the concentrations of Fe, Mn, Si and the alkalinity.

In the presence of CO_2, the concentration of Fe increases significantly to 5 mmol/L in the cleaned reservoir samples and to 3 mmol/L in the reservoir samples containing hydrocarbons, within the 83 days of the experiment (Figure 3.1 (a) and (b)). The presence of hydrocarbons seems to slow the release rate of Fe slightly. The release rate of Fe appears to be fastest in the beginning of the experiment, and although the release rate decreases with time, a constant concentration of Fe is not observed within the duration of the experiments. Measurements of both the total Fe and the Fe^{2+} concentrations with the Ferrozine method (Stookey, 1970) reveal that the concentration of total aqueous Fe equals that of aqueous Fe^{2+}. In contrast the Fe concentration remains close to 0 during the entire experiment in the absence of CO_2, hence the presence of CO_2 appears to initiate dissolution of Fe-bearing minerals.

The Mn concentration increases in the absence as well as in the presence of CO_2 (Figure 3.1 (c) and (d)), although the rate appears to be accelerated in the presence of CO_2. In the experiments with cleaned reservoir samples, comparable levels of Mn are released in both experiments reaching a concentration of 0.25 mmol/L. In the experiments with uncleaned samples a higher Mn concentration is observed at the end of the experiment as compared to the experiment without CO_2. For both experiments the concentration of Mn reaches a constant level in the presence of CO_2, whereas a continuous increase is observed in the absence of CO_2.

The alkalinity increases in all the experiments; however, a significant larger increase is observed in the experiments with CO_2 (Figure 3.1 (e) and (f)). Similar to the release of Fe, the increase in the alkalinity appears to be faster in the experiments with cleaned samples as compared to that in the reservoir samples containing hydrocarbons.

Also, the Si concentration increases in all the experiments, and while the same level is observed in the experiments without CO_2, a slightly higher Si concentration is observed in the experiments with CO_2 in the uncleaned samples.

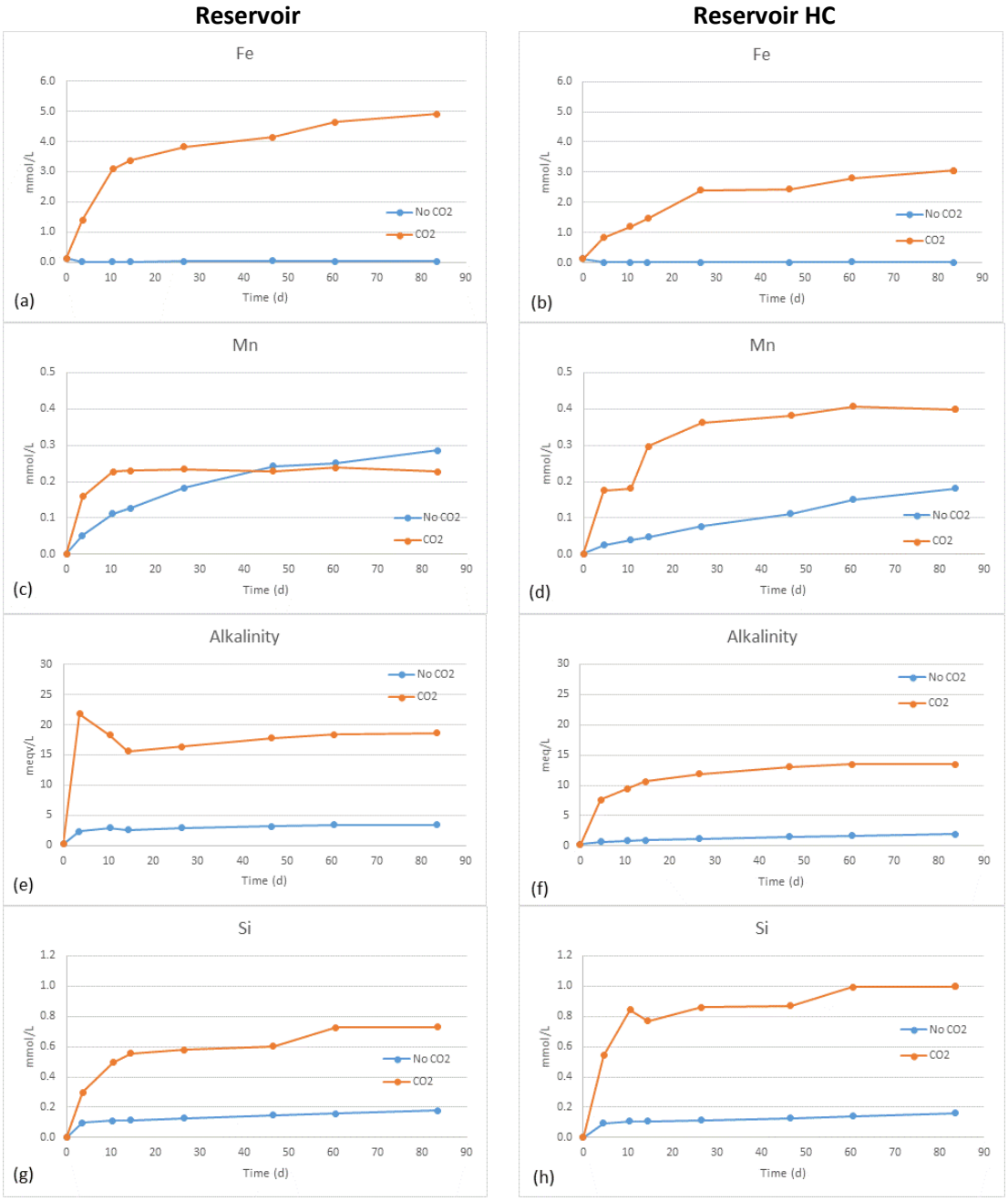

Figure 3.1 *Measured changes in the chemical composition of the brine during the experiment with cleaned reservoir samples (left) and reservoir samples containing hydrocarbons (right). Shown concentrations correspond to measurements at 25°C.* Brine composition is post experimental corrected as described in section 2.3.5.

Heavy metal release

The concentration of heavy metals released during the experiments are shown in Appendix 4. The figures show those components where the concentration deviates from 0. Appendix 4 shows that the presence of CO_2 may facilitate the release of Ce, Co, Li, Ni and P from the reservoir rock material.

3.1.2 Mineralogy and petrography prior to experiments

The composition of the sandstones used in the batch experiments is presented in Tables 3.1 and 3.2. Quartz is the dominant detrital grain (Table 3.1). Glauconite is typically rounded clasts which may have a slightly altered and occasionally fractured rim. Quartz occasionally has thick glauconitic coatings. K-feldspar is common, whereas plagioclase is rare. Glauconite has precipitated along crystallographic weakness zones in some K-feldspar grains. Phyllosilicates are minor detrital constituents. Muscovite is typically unaffected by diagenetic changes, though may have precipitation of calcite between the cleavage planes. Biotite is typically glauconitized in varying degree from thin intervals of glauconite between the cleavage planes to intensively expanded mica with weak lineation. Rock fragments of metamorphic, volcanic or granitic origin are rare. Heavy minerals comprise garnet, amphiboles, zircon, rutile, tourmaline, titanomagnetite, ilmenite altered to pseudorutile and leucoxene. Detrital clays occur as scattered pore filling matrix. The point counted detrital clays consists of a mixture of microquartz and Fe-and K- rich clays as revealed by SEM/EDS. Berthierine and mixed-layer smectite/illite are identified by XRD of the clay fraction (Table 3.3). Berthierine is identified as authigenic clays in other Nini samples (e.g. NI4A-1944.50) and hence less likely as a detrital component.

The dominant cementing phases comprise siderite, calcite/dolomite, K-feldspar and microquartz in decreasing abundances. Siderite occurs as rhombohedra in the pores in the sandstones. Siderite is typically zoned with an internal core of Mn-rich siderite and a thick rim of less Mn rich siderite ($(Fe_{0.65},Mn_{0.15},Ca_{0.10},Mg_{0.10})CO_3$). Carbonates occur as scattered micritic or poikilotopic cement. K-feldspar overgrowths are commonly optically discontinuous compared with the detrital K-feldspar. Microquartz coatings occur on detrital quartz grains and microquartz occurs as scattered crystal in detrital clays.

Table 3.1: Composition of sandstones based on point counting of thin sections.

	Quartz	K-feldspar	Plagioclase	Mica	Glauconite	Rock fragments	Heavy min.	Siderite	Other carbonate	Clays, detrital	Clays, authigenic	Other aut. phases	Porosity
NI4-1777.32	41.2	8.1	0.1	1.6	20.4	1.0	0.9	0.7	0.1	4.2	0.0	0.1	21.6
NI4-1777.27EX* **N_2**	40.7	5.5	0.4	1.1	21.7	0.2	0.7	0.7	0.0	5.6	0.0	0.5	23.5
NI4-1777.32EX	34.8	7.1	0.1	1.9	26.3	0.4	1.2	0.5	0.5	3.6	0.0	0.0	23.5
NI4-1779.19	37.2	10.4	0.3	0.9	24.3	0.5	0.9	0.6	0.6	4.7	0.0	0.0	19.6
NI4-1779.19EX **CO_2**	33.2	11.2	0.2	0.7	23.0	0.2	1.3	0.3	0.2	4.0	0.0	0.2	25.6
NI4-1779.32EX	33.2	10.0	0.2	1.9	23.5	0.3	0.9	0.5	0.0	5.1	0.0	0.0	24.5

*Loose sample, hence, point counting results highly uncertain (in particular porosity, which has been normalized to the other N_2 experiment sample)

Table 3.2: Composition of sandstones based on bulk-rock XRD.

Sample ID	Exp	Quartz	K-f	Plag.	Anatase	Pyrite	Barite	Calcite	Siderite	Chlorite	I+I/S	TOTAL
NI4-1777.27C		63.1	8.1	3.3	0.1	0.0	0.1	0.0	0.7	2.0	22.6	100
NI4-1777.32 EX	98 EX	63.2	7.0	3.4	0.1	0.1	0.0	0.0	0.4	3.2	22.6	100
NI4-1779.19C		63.5	7.6	3.3	0.2	0.0	0.1	0.0	0.7	1.9	22.7	100
NI4-1779.32 EX	104 EX	61.9	7.8	3.6	0.1	0.1	0.0	0.0	1.2	2.3	23.0	100

Table 3.3: Composition of clay fraction of the sandstones based on XRD.

Sample ID	Exp	Berthierine	Chlorite	Kaolinite	Illite	S/I	I+I/S	% Exp
NI4-1777.27C		4	-	-	3	93	-	70
NI4-1777.32 EX	98 EX	3	-	-	1	96	-	70
NI4-1779.19C		3	-	-	3	94	-	70
NI4-1779.32 EX	104 EX	2	-	-	2	97	-	70

3.1.3 Mineralogical changes during experiments

Mineralogical and petrographical changes in the sandstones after experiments comprise intensified partially dissolution of garnet (almandine), partial dissolution and alteration of siderite rhombs. K-feldspar overgrowths are unaffected by the experiments and show no dissolution or precipitation features (Figs 3.2, 34.). Garnet may show some dissolution features prior to the experiments; however, it is intensified in the experiment with uncleaned reservoir samples without CO_2.

Siderite rhombs are perfect prior to the experiment but show alteration and dissolution features after the experiments (Figs 3.2, 3.3, 3.4, 3.5). Siderite abundance decreases in all experiments compared with the initial composition (Table 3.2). Siderite crystals show clear dissolution features in the outermost rim of the crystals in the CO_2 experiments and to a lesser extend in the absence of CO_2 (Figs 3.2, 3.3, 3.4, 3.5). Precipitation of Fe-oxide/hydroxides around the initial outline of the siderite crystal is common in the CO_2 experiments and under the presence of hydrocarbons the Fe-oxide/hydroxides form thicker rims and enter secondary porosity in the rhombs (Figs 3.4, 3.5). Fe-oxide/hydroxide rims on siderite also form in the experiment without CO_2 under the presence of hydrocarbons. Scanning electron microscopy of the glauconitic sandstone confirms dissolution features in the siderite rim and precipitation of Fe-oxide/hydroxides.

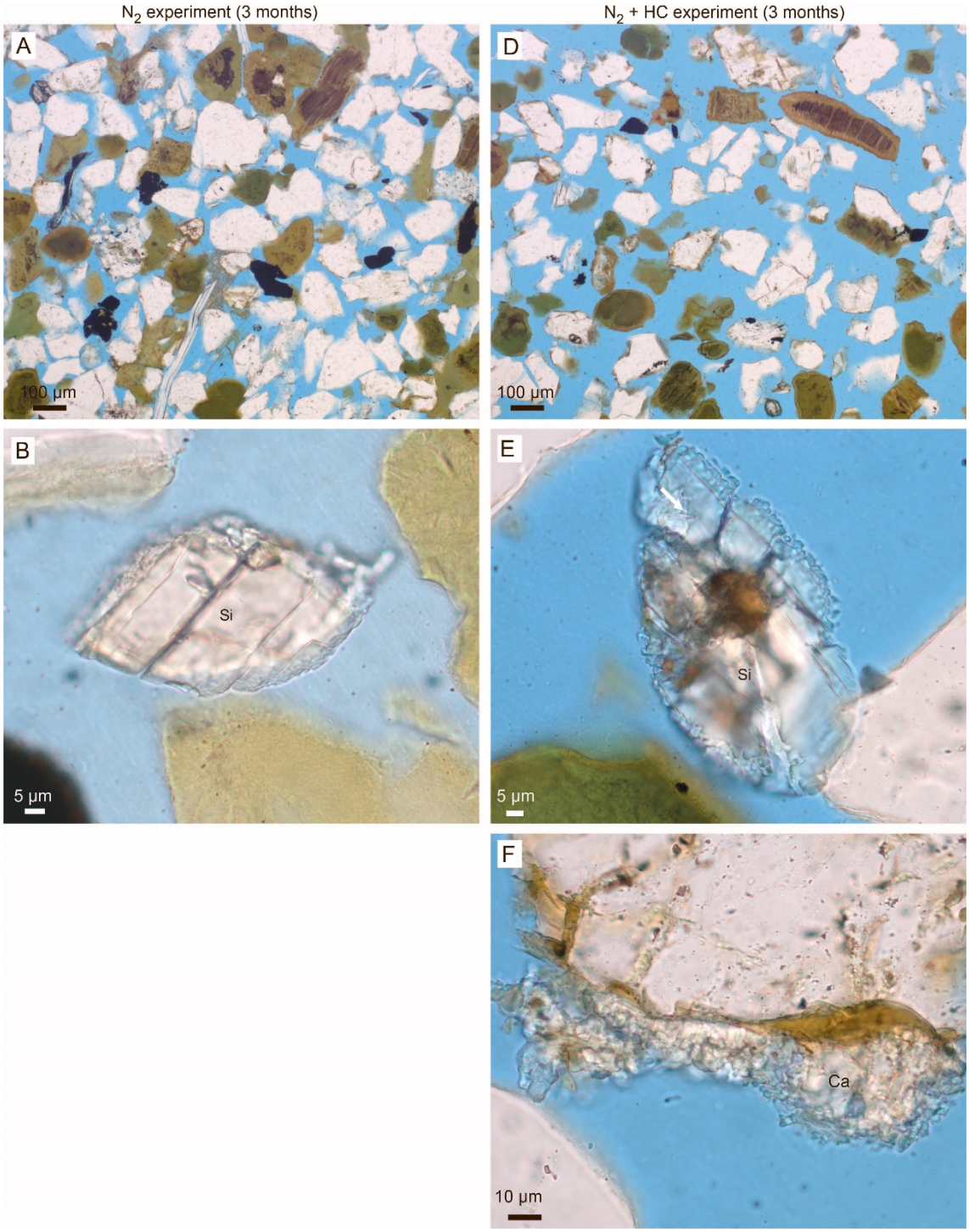

Figure 3.2: *Petrography of the glauconitic sandstone, NI4-1777.27EX, NI4-1777.32EX, applied in experiment without CO_2. A. Overview after no CO_2 experiment. B. Siderite (Si) with weak dissolution features. D. Overview of hydrocarbon-bearing (HC) sandstone after the no CO_2 experiment. E. Siderite (Si dissolution and precipitation of Fe-oxide/hydroxides. F. Partly dissolved calcite (Ca) cement.*

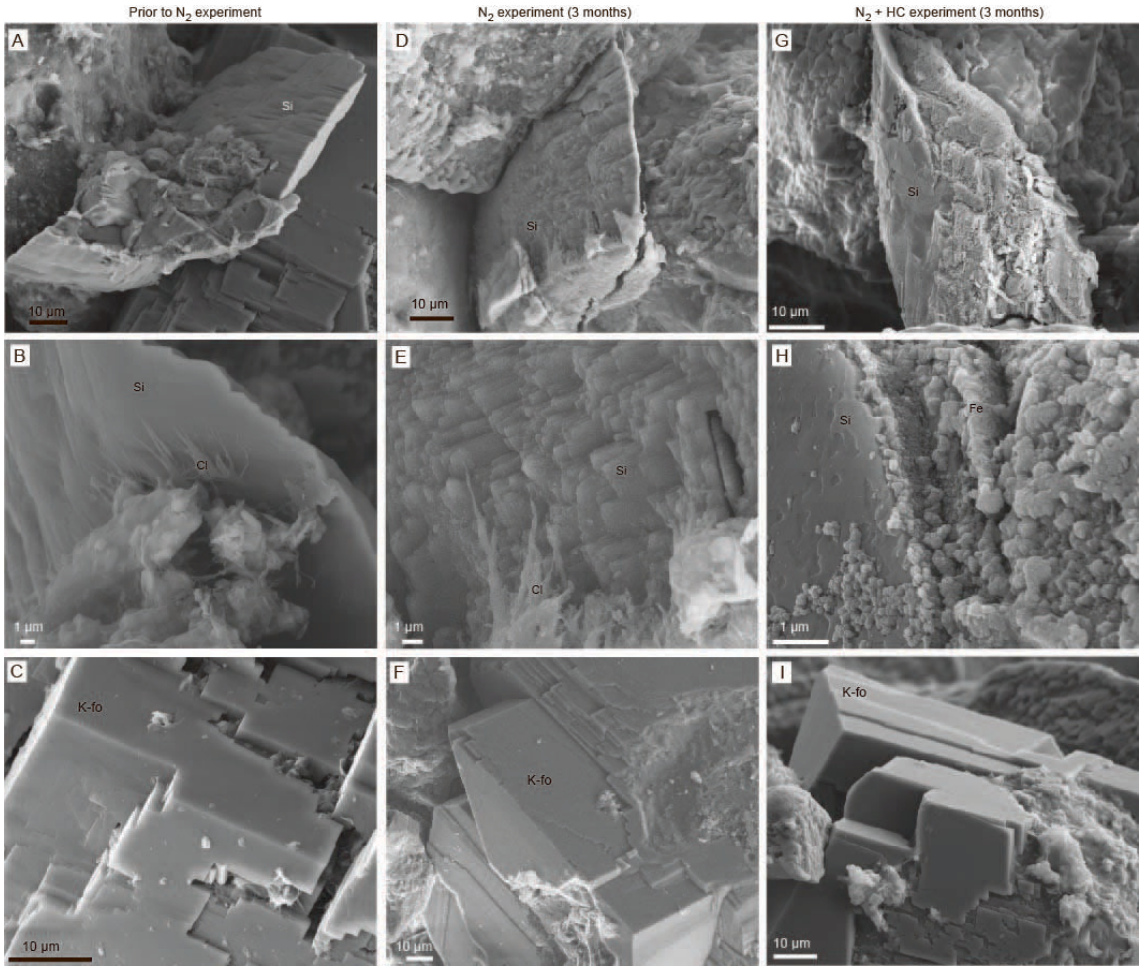

Figure 3.3: *Scanning electron micrographs (SE) of the glauconitic sandstone prior to experiment (NI4-1777.32, A, B, C), after no CO_2 experiment (NI4-1777.32EX, D, E, F) and under the presence of hydrocarbons (NI4-1777.27EX, G, H, I).* ***A.*** *Siderite (Si) crystal.* ***B.*** *Siderite (Si) coated with clays (Cl).* ***C.*** *K-feldspar overgrowth (K-fo).* ***D.*** *Siderite (Si) with dissolution features.* ***E.*** *Siderite (Si) with dissolution features, close up of D.* ***F.*** *K-feldspar overgrowth (K-fo) showing no effects of the experiment.* ***G.*** *Siderite (Si) with dissolution features and precipitation of Fe-oxide/hydroxides (Fe).* ***H.*** *Siderite (Si) with dissolution features and precipitation of Fe-oxide/hydroxides, close up of G.* ***I.*** *K-feldspar overgrowth (K-fo) showing no effects of the experiment.*

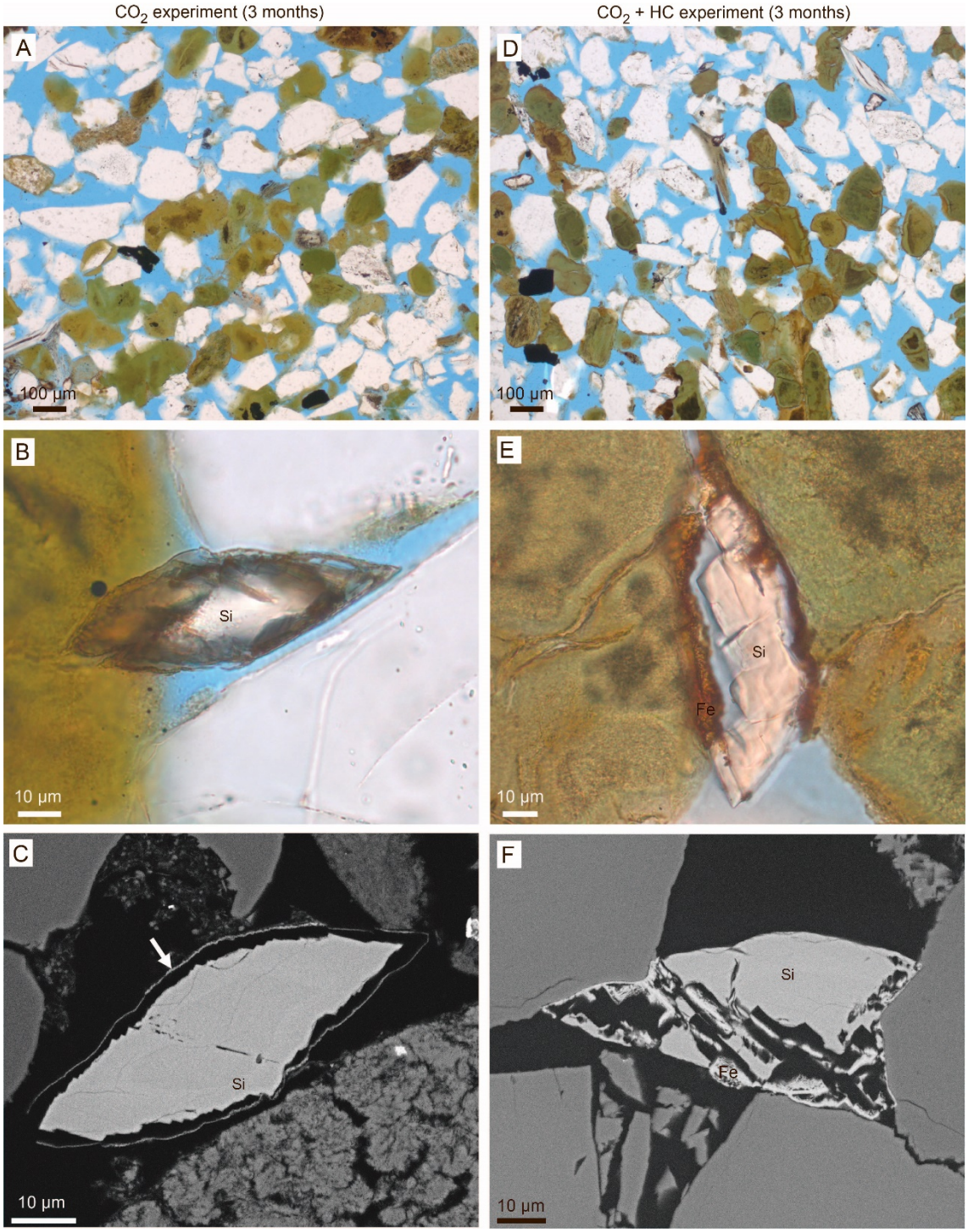

Figure 3.4: *Petrography of the glauconitic sandstone, NI4-1779.19EX, NI4-1779.32EX, applied in CO_2 experiment. A. Overview after CO_2 experiment. B. Siderite (Si) with weak dissolution features. C. Siderite (Si) with internal zonation due to variation in Mn and Mg contents and dissolution of the outermost part indicated by a rim of iron-oxide/hydroxides (arrow). Backscatter electron micrograph. D. Overview of hydrocarbon-bearing (HC) sandstone after CO_2 experiment. E. Siderite (Si) dissolution and precipitation of Fe-oxide/hydroxides. F. Siderite (Si) with dissolution features and precipitation of iron-oxide/hydroxides. Backscatter electron micrograph.*

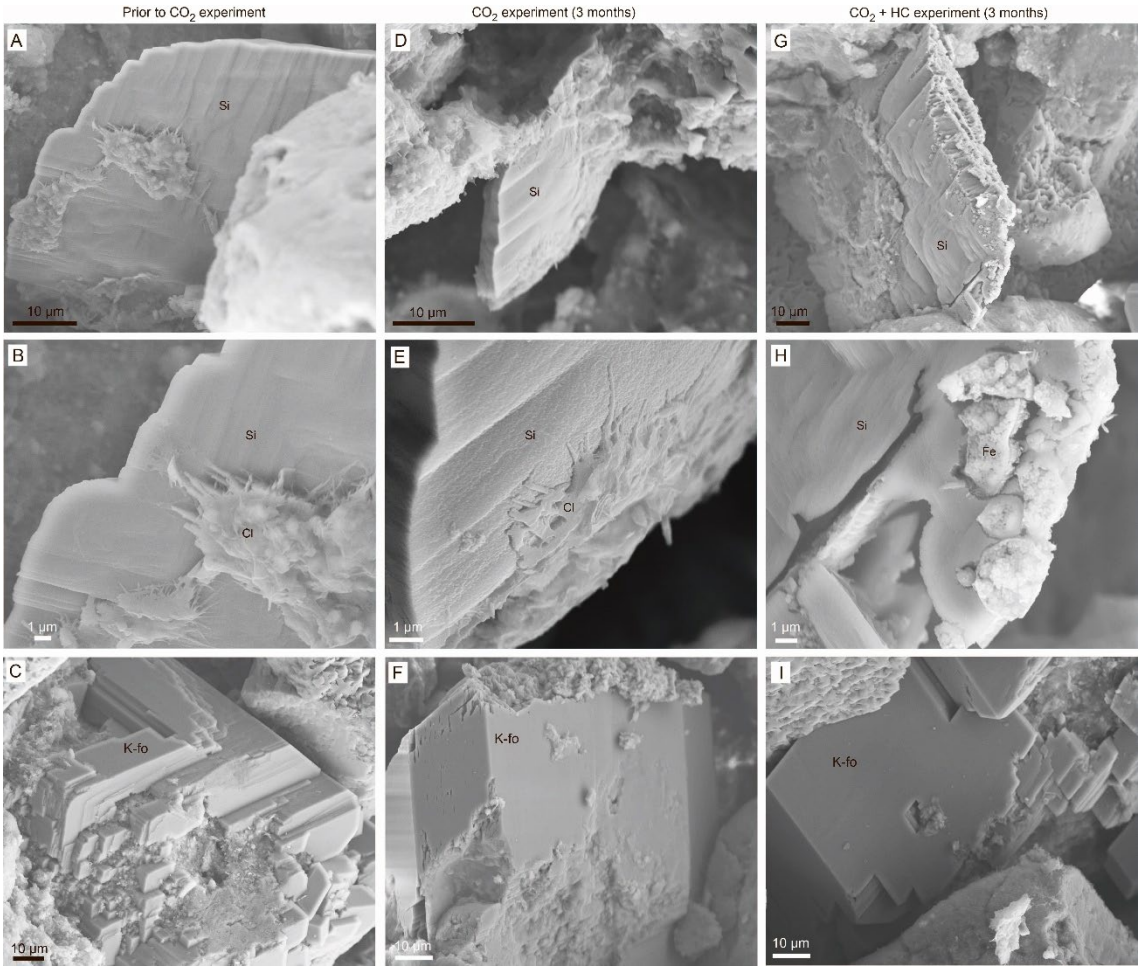

Figure 3.5: *Scanning electron micrographs (SE) of the glauconitic sandstone prior to experiment (NI4-1779.19, A, B, C), after CO_2 experiment (NI4-1779.32EX, D, E, F) and under the presence of hydrocarbons (NI4-1779.19EX, G, H, I).* ***A.*** *Siderite (Si) crystal.* ***B.*** *Siderite (Si) coated with clays (Cl).* ***C.*** *K-feldspar overgrowth (K-fo).* ***D.*** *Siderite (Si) without dissolution features.* ***E.*** *Siderite (Si) without dissolution features, close up of D.* ***F.*** *K-feldspar overgrowth (K-fo) showing no effects of the experiment.* ***G.*** *Siderite (Si) with dissolution features and precipitation of Fe-oxide/hydroxides (Fe).* ***H.*** *Siderite (Si) with dissolution features and precipitation of Fe-oxide/hydroxides, close up of G.* ***I.*** *K-feldspar overgrowth (K-fo) showing no effects of the experiment.*

3.1.4 Geochemical model

Based on the mineralogical changes observed during the experiments (cf. section 3.1.3) the geochemical model was fitted to the measured changes in the chemical composition of the brine during the experiments with the reservoir samples (Figure 3.1). An overview of the minerals included in the geochemical model mimicking the conditions in the experiments with reservoir samples is shown in Table 3.4 while the kinetic parameters applied in the models are shown in Appendix 5. Since the glauconite clasts consist of mixed-layer Fe-smectite/illite (Weibel et al., 2021), smectite is used in the model as a proxy for glauconite. The chemical formula for siderite is measured during the petrographic analysis in this study, while that of smectite and berthierine is taken from the literature (Blanc et al., 2012). The Mn^{2+} concentration is assumed to be controlled by the solubility of siderite. Thus, in order to fit the

modelled Mn^{2+} concentration to the measured concentration, the solubility of the Mn-containing siderite was slightly reduced (log (k) = -11.5 in the absence of CO_2 and log (k) = -10.63 in the presence of CO_2) compared to the solubility of clean siderite ($FeCO_3$, log (k) = -10.89) (Hörbrand et al., 2018). Alternatively, the relatively lower measured Mn-concentration at equilibrium could reflect deviations in the chemical composition of siderite.

The interaction between dissolution and precipitation processes of the minerals determines the chemical changes observed in the experiments. Although significant calcite dissolution cannot be confirmed by the petrographic analysis, the dissolution of calcite during the experiments is crucial to fit the modelled concentrations of the components of the carbonate system (pH, alkalinity and Ca) to the measured values.

The modelled and experimentally observed changes in the chemical composition of the brine for the experiments with cleaned reservoir samples are shown in Figure 3.6 and 3.7 in the absence and presence of CO_2, respectively. The results for the experiments with reservoir samples containing hydrocarbons are shown in Appendix 6.

Table 3.4 Overview of minerals included in the geochemical model fitted to the experimental data of the experiments with reservoir samples.

Mineral name	Chemical formula	Experiment	
		No CO_2	CO_2
Siderite	$Fe_{0.65}Mn_{0.15}Mg_{0.1}Ca_{0.1}CO3$	k	eq
Siderite_2[1)]	$FeCO_3$	n.i.	k
Calcite	CaCO3	eq	eq
Garnet	$Fe_3Al_2Si_3O_{12}$	k	k
Smectite	$Na_{0.409}K_{0.024}Ca_{0.009}(Si_{3.738}Al_{0.262})(Al_{1.598}Mg_{0.214}Fe_{0.208})O_{10}(OH)_2$	k	k
Berthierine[1)]	$(Si_{1.332}Al_{0.668})(Al_{0.976}Fe_{1.622}Mg_{0.157})O_5(OH)_4$	n.i.	k
Hematite	Fe_2O_3	eq	eq
$Al(OH)_3(a)$	$Al(OH)_3$	eq	eq

k: kinetic expression applied, eq: equilibrium assumed, n.i.: not included

[1)] Not included in the model for the experiments with reservoir samples in the absence of CO_2

Figure 3.6 shows that the experimentally obtained pH, alkalinity and the concentrations of Ca^{2+}, Fe^{2+}, Mn^{2+} and Si^{4+} are predicted reasonably well by the geochemical model for the cleaned reservoir samples in the absence of CO_2. The same trend is observed for the experiments with uncleaned reservoir samples in the absence of CO_2 (Appendix 5). Thus, the model predicts the slight decrease in the pH during the experiment, as well as the increase and general level of alkalinity, Ca^{2+} and Si^{4+}. Particularly for the Fe^{2+} concentration, the model

quite well predicts the initial decrease followed by a slight increase that reaches a constant level at *c.* 0.027 mmol/kgw.

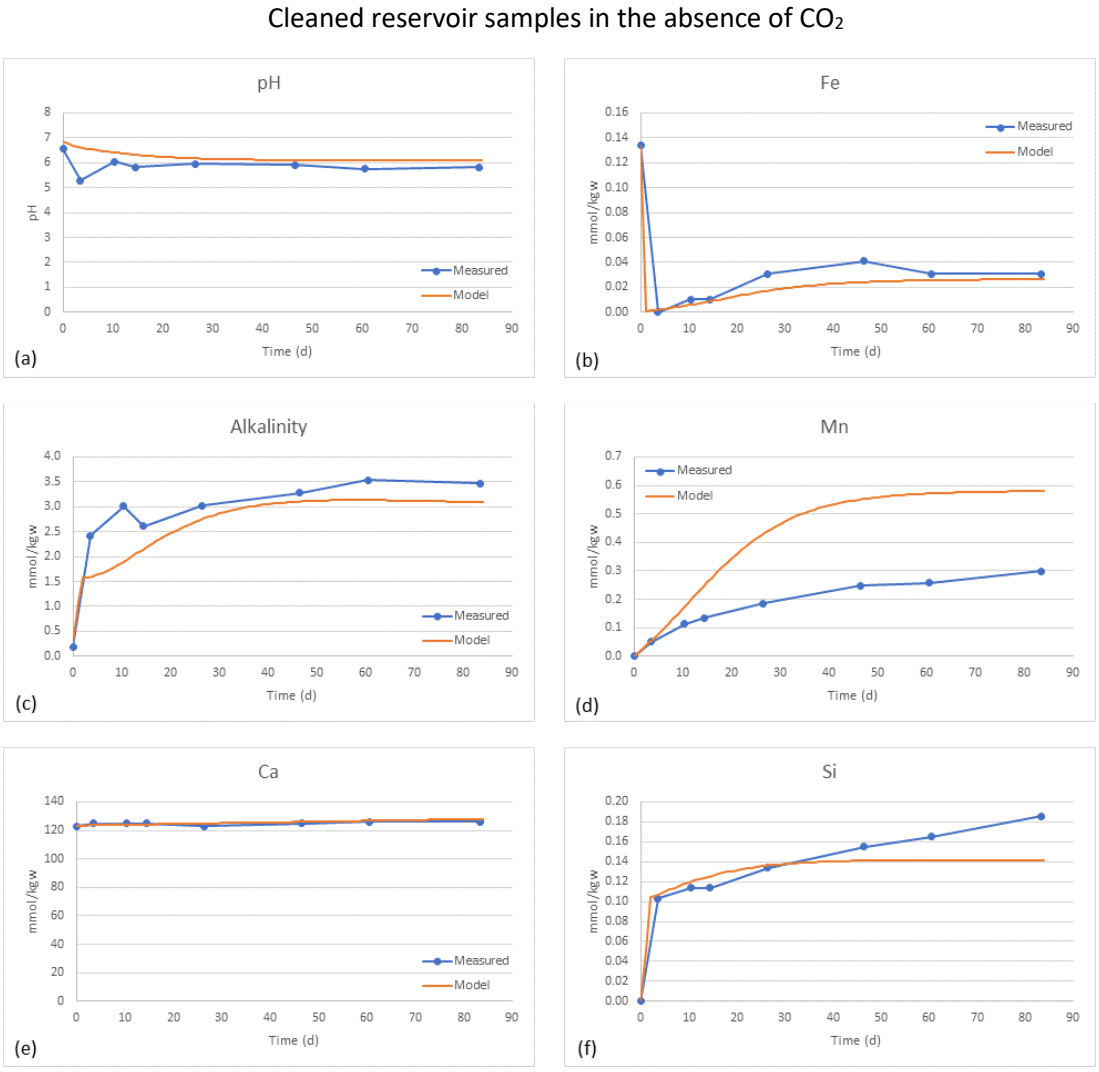

Figure 3.6 *Comparison of modelled and measured data for the experiment with cleaned reservoir samples in the absence of CO_2 (a) Calculated pH (60°C) based on pH measurements and modelled pH (60°C) for the experiment with reservoir material, (b) Fe concentration, (c) alkalinity, (d) Mn concentration (e) Ca concentration and (f) Si concentration.*

Similarly for the experiments with CO_2, the model predicts the experimentally obtained pH, alkalinity and the concentrations of Ca, Fe, Mn and Si reasonably well (Figure 3.7, appendix 5).

As described in section 2.3.2 the sampling procedure for the experiments with CO_2 involves a controlled degassing of CO_2 in a sampling cylinder and therefore numerical calculations were made to validate the consistency of the modelled and measured content of the CO_2 sensitive components pH, alkalinity and Ca (cf. section 2.3.4). Figure 3.7 shows that the best

fit of the modelled pH is obtained if calcite precipitation is not assumed to occur during the sampling procedure. In contrast, the best fit of the modelled alkalinity and Ca concentration is obtained if calcite precipitation is assumed. The pH is measured directly in the sampling cylinder whereas both the alkalinity and the Ca concentration is measured after extraction of the water sample from the sampling cylinder and filtration, cf. section 2.3.3. It is therefore likely that calcite precipitation occurs after the extraction of the water sample from the sampling cylinder and that any calcite particles are captured in the filtration process and therefore removed from the water sample prior to analysis resulting in a measured alkalinity and Ca concentration lower than that in the original water sample. This is in accordance with the fact that calcite precipitation was not detected in the sampling cylinder, cf. section 2.3.3.

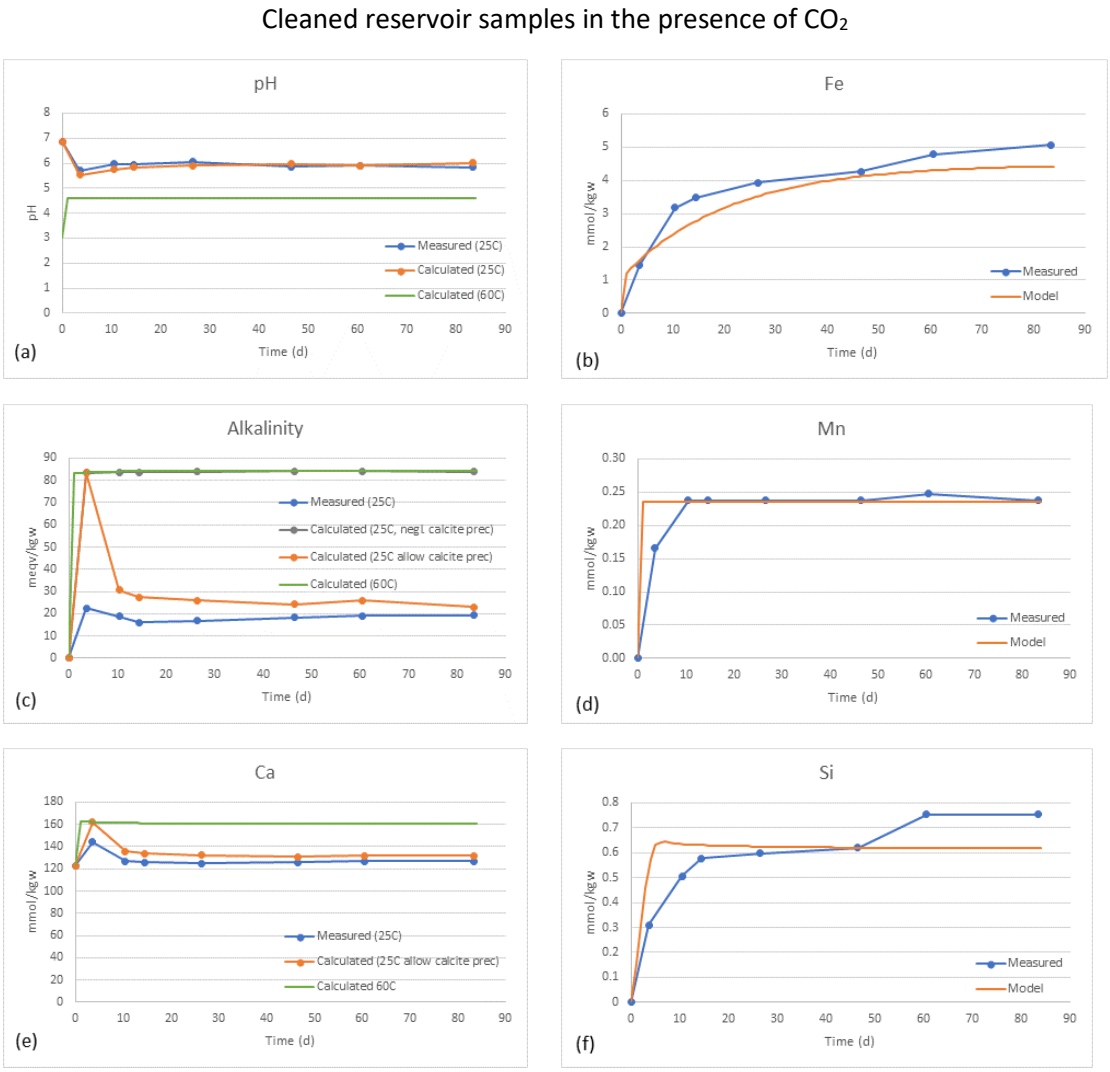

Figure 3.7 *pH measurements (at 25°C) and calculated pH (at 25°C and 60°C) for the experiment with reservoir material (a), alkalinity determinations (at 25°C) and calculations (at 25°C neglecting and allowing precipitation of calcite prior to alkalinity determination and at 60°C) (c), and measured calcium concentration at 25°C, calculated calcium concentration (25°C) assuming precipitation of calcite prior to filtration of the water sample and at 60°C for the experiment with reservoir material (e) and measured and modelled concentrations of Fe (b), Mn (d) and Si (f).*

Since the modelled changes in the chemical composition of the brine fit reasonably well with the experimental data, it is fair to assume that the model predicts the geochemical reaction during the experiments adequately. Figure 3.8 illustrates the minerals that either dissolves or precipitates during the experiments with reservoir samples.

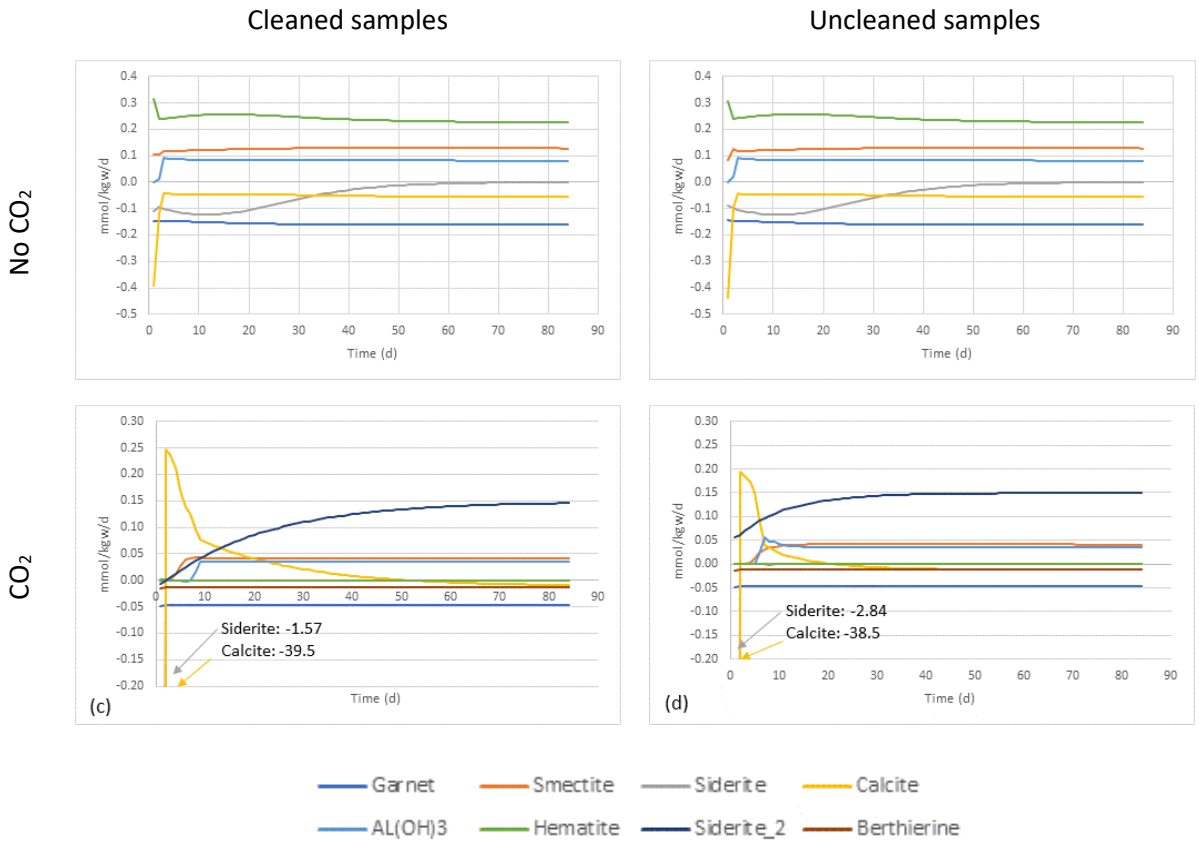

Figure 3.8: *Rate of mineral dissolution (negative value) or precipitation (positive value) as predicted by the geochemical model in the experiments with cleaned (left column) and uncleaned (right column) reservoir samples in the absence (top row) and presence (bottom row) of CO_2. A positive value indicates that the mineral precipitates while a negative value indicates that the minerals dissolves. Note the difference in the scale.*

3.1.5 Hydrogeochemical reactions in the absence of CO_2

The geochemical models for the experiments with and without hydrocarbons predict similar dissolution/precipitation reactions between the Paleocene sandstone reservoir of the Nini West Field and the brine in the absence of CO_2 (Figure 3.8). Hence, the presence of hydrocarbons is not expected to affect the dissolution/precipitation processes between the Paleocene sandstone reservoir of the Nini West Field and the brine applied in the experiments.
In the absence of CO_2, siderite dissolution occurs within the first *c.* 60 days of the experiment after which equilibrium with siderite is reached and the dissolution ceases (Figure 3.8). A large dissolution of calcite occurs momentarily at the beginning of the experiment after which

the rate of calcite dissolution decreases rapidly, and a continuous dissolution takes place in the rest of the experiment. Additionally, a continuous dissolution of garnet takes place throughout the experiment releasing Fe to the solution. Some of the Fe is reprecipitated as smectite and hematite. This involves a change in the oxidation state of Fe from Fe(II) to Fe(III). It is currently uncertain which reaction facilitate this oxidation of Fe(II). There is, however, no indication that this is caused by intrusion of oxygen during the experiments.

Table 3.5 Overview of mineralogical changes during the experiments without CO_2 present, based on mass balances of the model output.

		Cleaned samples		Uncleaned	
	Composition start	Composition end	Fraction of mineral reacted	Composition end	Fraction of mineral reacted
	(vol%)	(vol%)	(%)	(vol%)	(%)
Quartz	41.2	41.2	n.i.	41.2	n.i.
K-feldspar	8.1	8.1	n.i.	8.1	n.i.
Plagioclase	0.1	0.1	n.i.	0.1	n.i.
Mica	1.6	1.6	n.i.	1.6	n.i.
Rock fragments	1.0	1.0	n.i.	1.0	n.i.
Heavy min. (Garnet)	0.9	0.8	4.4	0.8	4.4
Siderite	0.7	0.7	0.4	0.7	0.4
Other carbonate (Calcite)	0.1	0.1	2.4	0.1	2.4
Smectite incl. glauconite	16.9	16.9	0.2	16.9	0.2
Berthierine	0.5	0.5	n.i.	0.5	-0.5
Illite	7.2	7.2	n.i.	7.2	n.i.
Clays, authigenic	0.0	0.0	n.i.	0.0	n.i.
Other aut. Phases	0.1	0.1	n.i.	0.1	n.i.
Porosity	21.6	21,6		21.6	
Sum	100	100		100	

Great effort was made to approximate the brine used in the experiments with the formation water in the reservoir. The formation water has equilibrated with the reservoir rock material for millions of years, and therefore only very limited reactions between the formation water and the reservoir rock is expected in the absence of CO_2. The fact that we do see evolution in the mineral composition and water composition in the experiments with the brine in the absence of CO_2 suggests; 1) the P50 composition used to define the brine is from produced water from the Nini field and not specifically from the Nini 4 well, 2) analytical uncertainties

exist with respect to measuring water at surface conditions from a production stream – we inferred that the measured alkalinity and Ba that both showed supersaturation were in error 3) unmeasured components (e.g. Si) in the produced water or mineral solubility temperature variations makes it very difficult to produce the exact brine in the laboratory 4) the specific samples mineralogical composition might be at odd with the general reservoir composition 5) the sample preparation might have exposed and crushed grains thereby creating reactive parts that not else will be exposed in the reservoir. Therefore, one could argue that the water composition measured in the end of the experiments offers a better answer to what starting composition of the water should have been in order to avoid un-need mineral reactions.

3.1.6 Hydrogeochemical reactions in the presence of CO_2

Similarly, to the experiments without CO_2, the presence of hydrocarbons does not seem to affect the nature of the dissolution/precipitation processes between the Paleocene sandstone reservoir of the Nini West Field and the brine in the presence of CO_2 (Figure 3.8). The rate of some of the processes may vary slightly, which may be attributed to heterogeneities in the core material or that the hydrocarbons may block some of the reactive sites on the minerals.

The most prominent reaction in the presence of CO_2 is the initial dissolution of calcite (Figure 3.8) caused by the lowering of the pH by the CO_2. The dissolution of calcite buffers the pH, and although not detected by the petrographic analysis, the calcite dissolution is very important in controlling the pH, alkalinity and Ca concentration. After the initial dissolution, calcite reprecipitates with a decreasing rate for the rest of the experiment. Still, a net dissolution of calcite occurs in the experiment and mass balance calculations show that *c.* 23% of the calcite dissolves during the experiment (Table 3.6).

Additionally, siderite dissolves initially, but not to the same degree as calcite. While siderite dissolution appears to be kinetically controlled in the absence of CO_2, the siderite dissolution rate is accelerated in the presence of CO_2. Hence, the concentration of the aqueous species can satisfactorily be described by assuming that siderite dissolution is controlled by equilibrium. In the presence of CO_2, the measured Fe concentration exceeds that of siderite equilibrium, and therefore kinetically controlled precipitation of siderite is assumed. The constant Mn concentration indicates, however, that a Mn phase does not reprecipitate and therefore a “pure” ($FeCO_3$) siderite is assumed to precipitate. This reprecipitation of an Mn-free siderite is essential to be able to fit both the Fe and Mn concentrations. The model predicts that 0.1% of the siderite initially present in the reservoir sample dissolves, while a net precipitation corresponding to 0.8% of the siderite originally present in the sample precipitates.

Table 3.6 Overview of mineralogical changes during the experiments with CO_2 present, based on mass balances of the model output.

		Cleaned samples		Uncleaned samples	
	Composition start	Composition end	Fraction of mineral reacted	Composition end	Fraction of mineral reacted
	(vol%)	(vol%)	(%)	(vol%)	(%)
Quartz	37.2	37.2	n.i.	37.2	n.i.
K-feldspar	10.4	10.4	n.i.	10.4	n.i.
Plagioclase	0.3	0.3	n.i.	0.3	n.i.
Mica	0.9	0.9	n.i.	0.9	n.i.
Rock fragments	0.5	0.5	n.i.	0.5	n.i.
Heavy min. (Garnet)	0.9	0.9	1.3	0.9	1.3
Siderite	0.6	0.6	0.8	0.6	0.8
Other carbonate (Calcite)	0.6	0.6	23	0.6	24
Smectite incl. glauconite	19.9	19.9	0.05	19.9	0.05
Berthierine	0.5	0.5	0.5	0.5	0.5
Illite	8.5	8.5	n.i.	8.5	n.i.
Clays, authigenic	0.0	0.0	n.i.	0.0	n.i.
Other aut. Phases	0.0	0.0	n.i.	0.0	n.i.
Porosity	19.6	19.6		19.6	
Sum	100	100		100	

As in the experiments without CO_2, garnet is continuously dissolved while smectite precipitates, however, to a lesser extent in the experiments with CO_2. Thus only c. 1% of the initially garnet present in the reservoir sample dissolves during the experiment. Hematite only precipitates to a lesser extend in the first *c.* 4 days of the experiment. An additional Fe rich source was needed in the model for the experiments with reservoir samples in the presence of CO_2 in order to fit the Fe concentration, and therefore berthierine was included in the model. Since the kinetic parameters for berthierine dissolution to the best of our knowledge is unknown, kinetic parameters for berthierine dissolution is assumed equal to those of chlorite. Approximately 0.5% of the berthierine is predicted to dissolve.

To sum up: compared to the experiments without CO_2, the presence of CO_2 leads to a significant increase in the initial dissolution of calcite. In the presence of CO_2, calcite dissolution is followed by precipitation of calcite for the rest of the experiment, while calcite dissolution continuous throughout the experiments without CO_2. Additionally, the presence of CO_2 leads to an increase in the dissolution of Mn-bearing siderite followed by precipitation of a Mn lean

"pure Fe" siderite. Reprecipitation of siderite does not take place in the absence of CO_2. Furthermore, the CO_2 induces the dissolution of an additional Fe-containing mineral, presumably berthierine. The dissolution of garnet and precipitation of smectite is reduced while hematite precipitation is suppressed in the experiments with CO_2.

An overview of the mineralogical changes during the experiments without and with CO_2 is shown in Table 3.5 and 3.6, respectively. Both tables illustrate that only insignificant changes in the mineralogical composition of the reservoir rock occur during the experiments.

3.2 Seal

3.2.1 Measured changes in brine composition

The effect of CO_2 reactions with the seal overlying the Paleocene sandstone reservoir of the Nini West Field is shown in Figure 3.9. Raw data not post experimental corrected (cf. section 2.3.5) are illustrated in Appendix 3. Similar to the experiments with the reservoir material, significant increases are observed for the concentrations of Fe, Mn, Si and the alkalinity. For all these components, a significant higher concentration is observed in the experiments with CO_2 as compared to that in the experiments without CO_2. While a continuous increase in the concentration of Fe is observed in the presence of CO_2, both the concentrations of Mn, Si and alkalinity appears to reach a constant level. For all measurements, the aqueous concentration of total Fe equals that of Fe^{2+}.

Heavy metal release

The concentration of heavy metals released during the experiments with the seal material are shown in appendix 4. The figures show those components where the concentration deviates from 0. Appendix 4 shows that the presence of CO_2 may facilitate the release of Ce, Co, Cr, Ni, P, and Zn from the reservoir rock material. Additionally, Li and Rb are released in comparable concentrations in the presence and in the absence of CO_2.

Seal

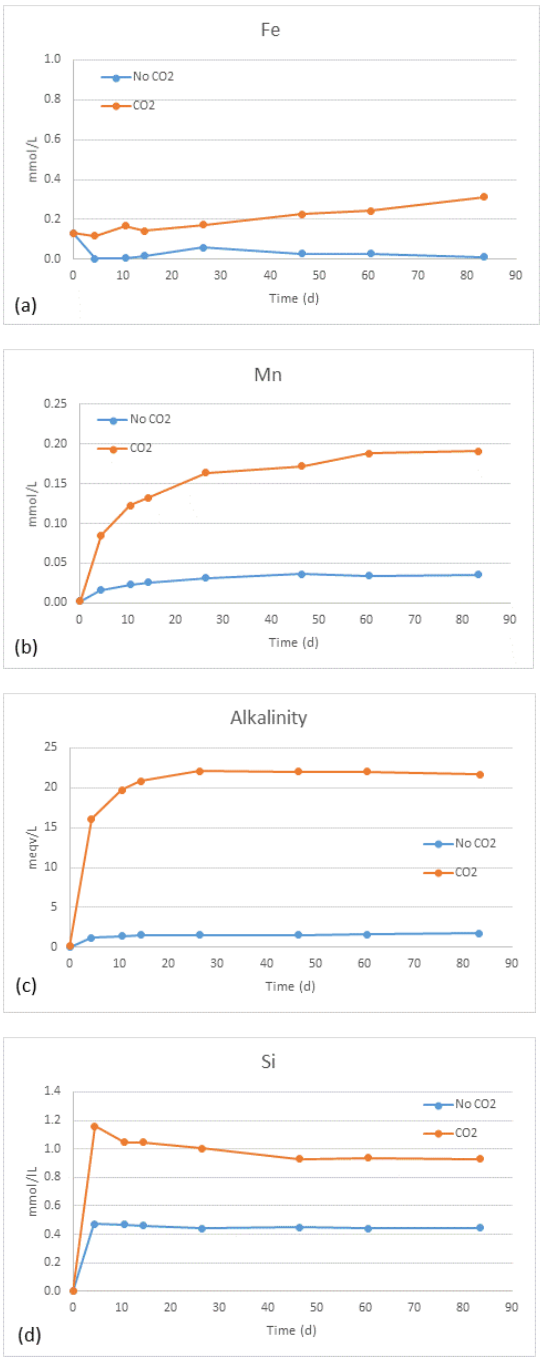

Figure 3.9 *Measured changes in the chemical composition of the brine during the experiment seal samples. Shown concentrations correspond to measurements at 25°C. Measurements are post experimental corrected as described in section 2.3.5.*

3.2.2 Mineralogy and petrography prior to experiments

The composition of the mudstone samples from the Nini-4 well are presented in Table 3.7. The mudstone consists of a clay matrix of illite and smectite, besides scattered quartz and feldspar silt-sized grains. Pyrite occurs as framboids associated with organic material. Heulandite fills sand-sized (up to 200 µm) secondary porosity probably after diatoms. The composition of heulandite was evaluated by SEM/EDS to be a sodium-dominant variety $(Na)_{2-3}Al_3(Al,Si)_2Si_{13}O_{36} \cdot 12(H_2O)$ i.e. with a similar composition as clinoptilolite. Heulandite encloses tiny spheres of opal and areas of iron-rich clay minerals and microquartz.

Table 3.7: Composition of seal samples based on bulk-rock XRD.

Sample No.	Plug	Lab	Quartz (%)	Plag. (%)	Siderite (%)	Pyrite (%)	Heulandite (%)	Muscovite / illite (%)	Smectite (%)
NI4-1748.65	15	DTU / RWH	14.6	2.5	3.9	1.1	11.4	37.7	28.7
NI4-1748.65	**15**	**KU / Tonci**	**20.2**			**1.1**	**19.3**	**30.8**	**28.6**
NI4-1748.70EX	**15 C**	**KU / Tonci**	**20.6**			**1.2**	**19.0**	**33.0**	**26.7**
NI4-1749-1755		DTU / RWH	14.0	2.9	3.7	1.5	17.5	21.8	38.6
NI4-1762.27	95	DTU / RWH	15.5	2.1	3.8	2.6	23.6	20.4	31.9
NI4-1762.27	**95**	**KU / Tonci**	**26.1**			**1.9**	**24.5**	**18.3**	**29.2**

Table 3.8: Composition of the clay fraction of the seal samples based on XRD.

Sample ID	Exp	Berthierine	Chlorite	Kaolinite	Illite	S/I	I+I/S	% Exp
NI4-1748.65	15	-	1	trace	6	93	-	90
NI4-1748.70 EX	15C EX	-	trace	trace	4	96	-	90
NI4-1748.65 EX	15 EX	-	1	trace	6	93	-	90

3.2.3 Mineralogical changes during experiments

XRD results show a slight increase in illite and comparable decrease in smectite after the CO_2 experiment (compare NI4-1748.65 with NI4-1748.65EX in Table 3.7). Smectite is a randomly stratified mixed-layer smectite/illite (Table 3.8). Transformation of smectite-layers into illite-layers cannot be verified by the mineralogical composition of the clay fraction.

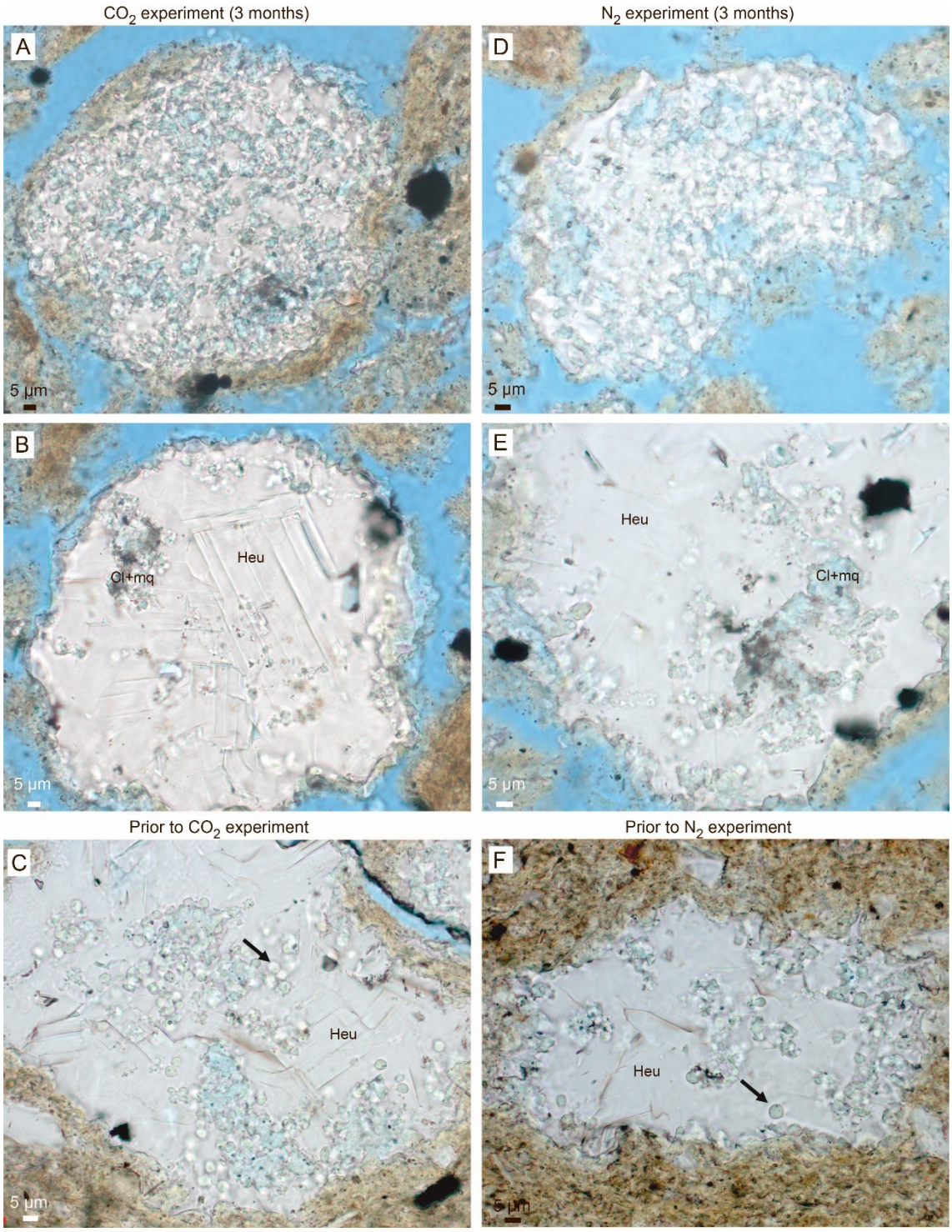

Figure 3.10: *Heulandite-filling (Heu) of secondary porosity after diatoms in transmitted light after CO_2 experiment (A, B), after the no CO_2 experiment (D,E) and prior to experiments (C, F). A. Heulandite with dissolution voids. B. Interlocking heulandite crystals with pores filled by Fe-rich clays (Cl) and microquartz (mq). C. Heulandite enclosing opal spheres (arrow). D. Heulandite with dissolution voids. E. Interlocking heulandite crystals with pores filled by Fe-rich clays (Cl) and microquartz (mq). F. Heulandite enclosing opal spheres (arow).*

Heulandite-filled secondary porosity after diatom frustules can vary in appearance after experiments. Some show clear dissolution voids (Fig. 3.10A, D), whereas other seems to be unaffected by the alteration (Fig. 3.10B, E). Prior to the experiments, heulandite enclose opal spheres (Fig. 3.10C, F). Opal spheres are not observed in samples applied in the experiment. Consequently, opal was probably dissolved during the experiments and alteration may have continued inwards from the location of weakness.

3.2.4 Geochemical model

The mineralogical changes observed during the experiments (cf. section 3.2.3) serve as input to the geochemical model. The model was subsequently calibrated by fitting the model output to the measured changes in the chemical composition of the brine during the experiments with the seal samples (Figure 3.9). Due to the limited mineralogical changes observed by the petrographic analysis, the geochemical model for the seal is less constrained than that for the reservoir, and therefore associated with larger uncertainties.

An overview of the minerals included in the geochemical model for the experiments with samples of the seal overlying the Paleocene sandstone reservoir of the Nini West Field is shown in Table 3.9 while the kinetic parameters applied in the models are shown in Appendix 5.

The same chemical formula is applied for siderite in the seal as in the reservoir (cf. section 3.1.2) while the chemical formula of heulandite is found in the in the literature, applying that of a Na-rich heulandite (Blanc et al., 2012). Chalcedony is used in the model as a proxy for opal. The better fit was obtained by increasing the solubility of chalcedony slightly from log(k) = -3.55 to log(k) = -3.15. In order to fit both the Fe and the Mn concentrations an additional mineral source of Mn besides siderite is needed in the model, and therefore equilibrium with rhodochrosite ($MnCO_3$) is assumed. This could also reflect that the siderite in the seal has a different chemical formula that siderite that reside in the reservoir.

The modelled and experimentally observed changes in the chemical composition of the brine for the experiments with cleaned reservoir samples are shown in Figure 3.6 and 3.7 in the absence and presence of CO_2, respectively.

Table 3.9 Overview of minerals included in the geochemical model fitted to the experimental data of the experiments with seal samples.

Mineral name	Chemical formula	Experiment	
		No CO_2	CO_2
Siderite	$Fe_{0.65}Mn_{0.15}Mg_{0.1}Ca_{0.1}CO_3$	eq	eq
Chalcedony	SiO_2	eq	eq
Heulandite	$Na_{2.14}Al_{2.14}Si_{6.86}O_{18}$:6.17$H_2O$	k	K
Calcite	CaCO3	n.i.	eq
Rhodochrosite	$MnCO_3$	n.i.	eq
Hematite	Fe_2O_3	eq	eq
Illite	$K_{0.85}Fe_{0.25}Al_{2.35}Si_{3.4}O_{10}(OH)_2$	n.i.	k

k: kinetic expression applied, eq: equilibrium assumed, n.i.: not included

[2)] Not included in the model for the experiments with seal samples in the absence of CO_2

Figure 3.11 shows that the experimentally obtained pH, alkalinity and the concentrations of Ca, Fe, Mn and Si are predicted reasonably well by the geochemical model for the seal samples in the absence of CO_2. Thus, the model predicts the pH, and the Si, Ca and Mn concentrations reasonably well. The model overestimates the alkalinity and does not predict the increase in the Fe concentration followed by a decrease as well as overestimates the alkalinity slightly. Particularly for the Fe concentration, the measured concentration is lower than calculated and therefore associated with some uncertainty.

For the experiments with CO_2, the model predicts the experimentally obtained pH, alkalinity and the concentrations of Ca, Fe, Mn and Si reasonably well (Figure 3.12). As described in section 2.3.2 the sampling procedure for the experiments with CO_2 involves a controlled de-gassing of CO_2 in a sampling cylinder and therefore numerical calculations were made to validate the consistency of the modelled and measured content of the CO_2 sensitive components pH, alkalinity and Ca (cf. section 2.3.4). As for the results for the reservoir samples, the results shown in Figure 3.12 indicate that calcite precipitates during the sampling procedure after the extraction of the water sample from the sampling cylinder and that any calcite particles are captured in the filtration process (cf. section 3.1.4).

Figure 3.11 illustrates the minerals that either dissolves or precipitates during the experiments with seal samples as predicted by the geochemical model calibrated towards the experimental data. Generally, the seal appears less reactive than the reservoir.

Seal samples in the absence of CO_2

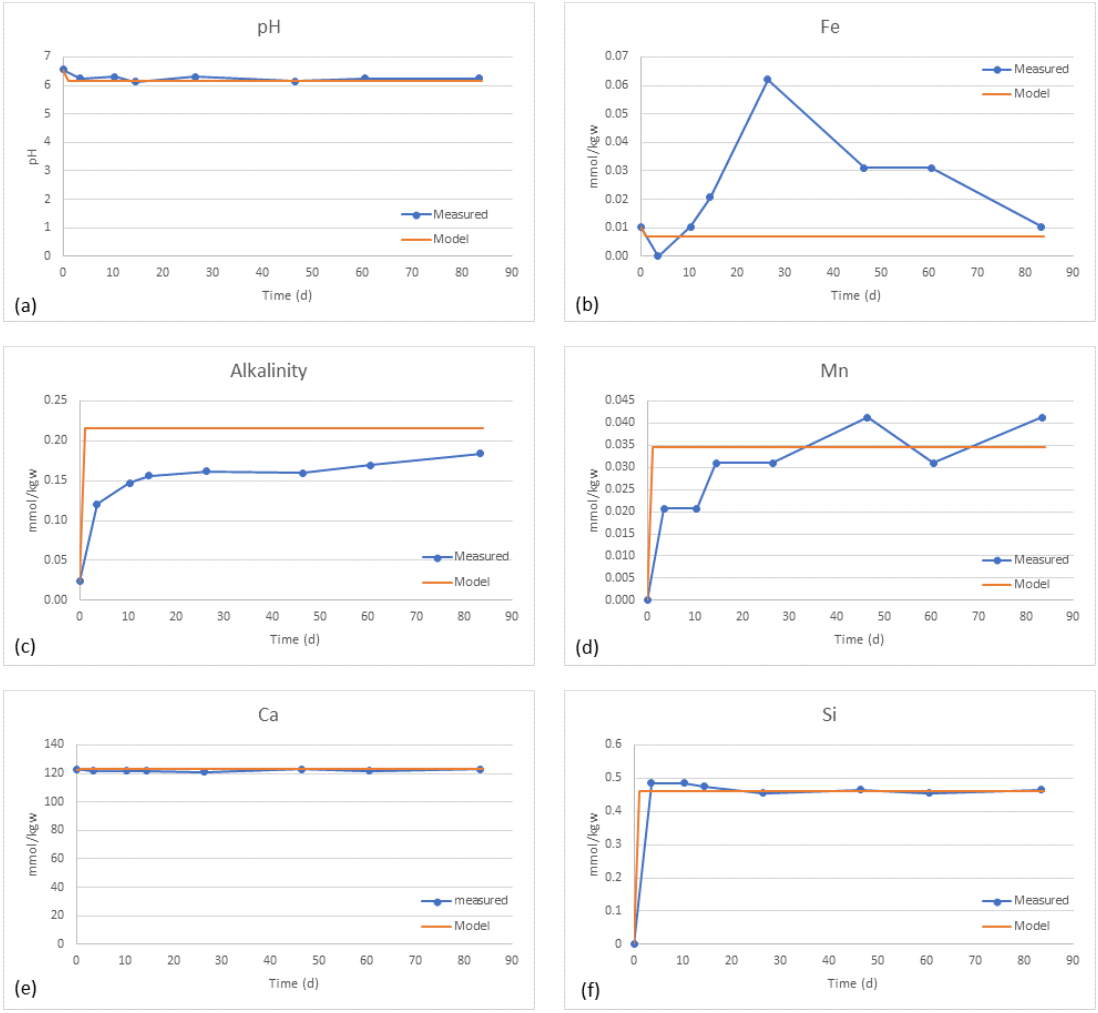

Figure 3.11 *Comparison of modelled and measured data for the experiment with seal samples in the absence of CO_2 (a) Calculated pH (60°C) based on pH measurements and modelled pH (60°C) for the experiment with reservoir material, (b) Fe concentration, (c) Alkalinity, (d) Mn concentration (e) Ca concentration and (f) Si concentration.*

Seal samples in the presence of CO_2

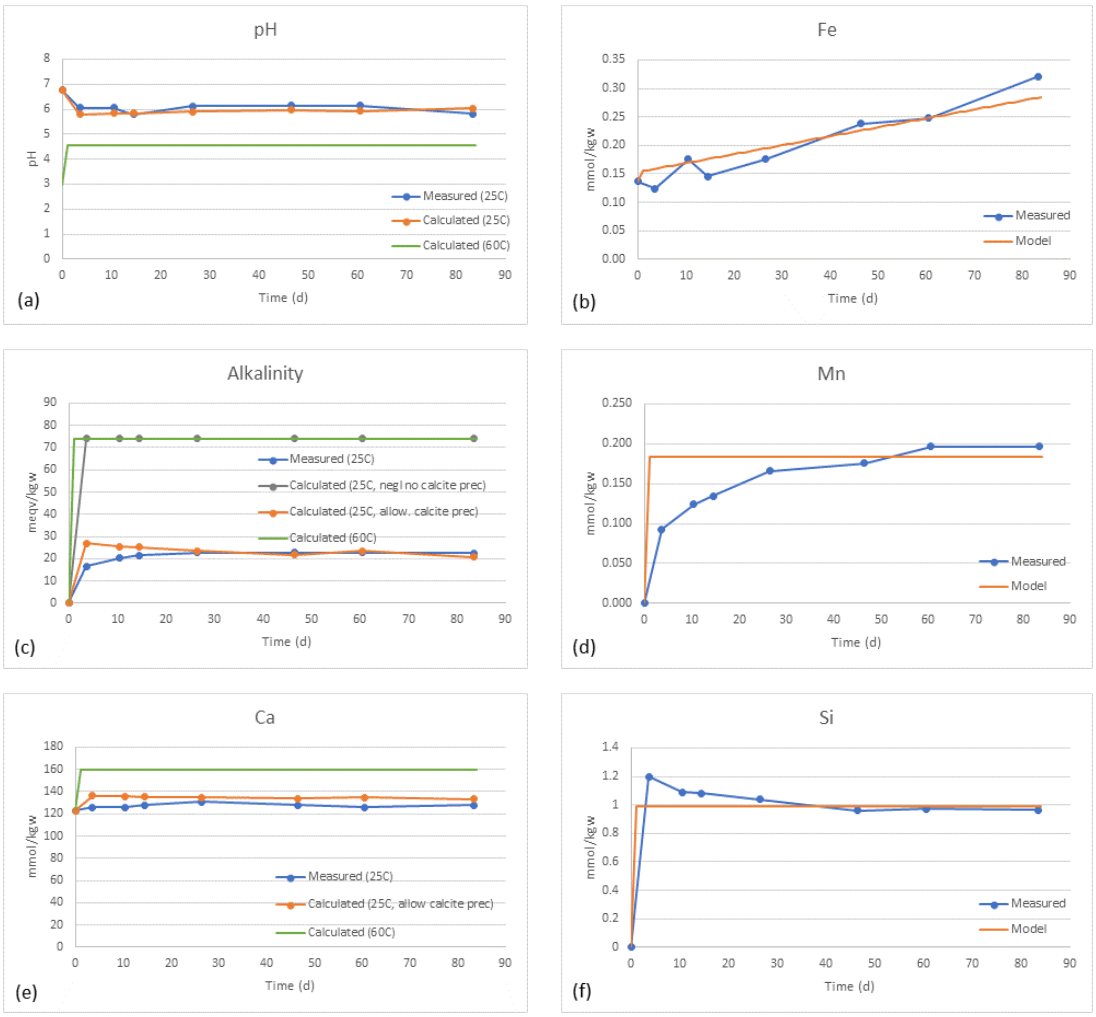

Figure 3.12 *pH measurements (at 25°C) and calculated pH (at 25°C and 60°C) for the experiment with seal material (a), alkalinity determinations (at 25°C) and calculations (at 25°C neglecting and allowing precipitation of calcite prior to alkalinity determination and at 60°C) (c), and measured calcium concentration at 25°C, calculated calcium concentration (25°C) assuming precipitation of calcite prior to filtration of the water sample and at 60°C for the experiment with reservoir material (e) and measured and modelled concentrations of Fe (b), Mn (d) and Si (f).*

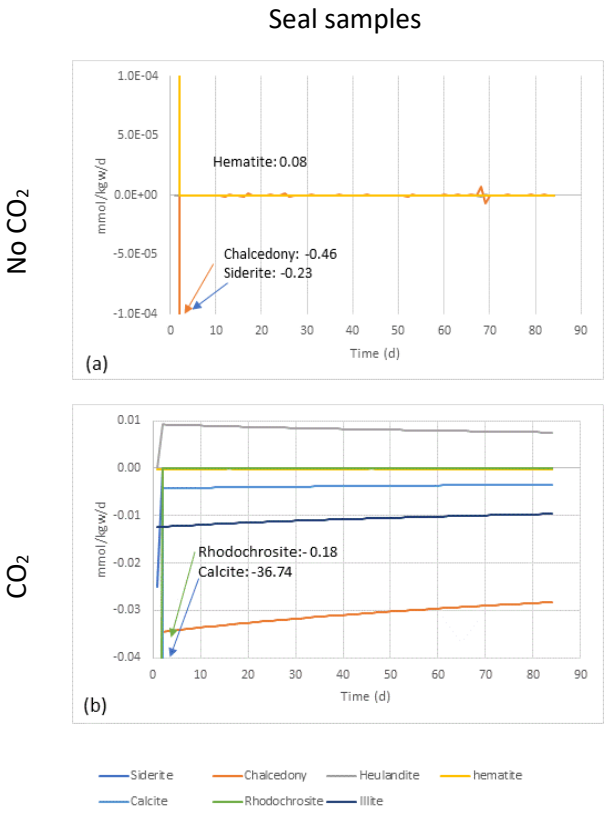

Figure 3.8*: Rate of mineral dissolution (negative value) or precipitation (positive value) as predicted by the geochemical model in the experiments with seal samples in the absence (top row) and presence (bottom row) of CO_2. A positive value indicates that the mineral precipitates while a negative value indicates that the minerals dissolves. Note the difference in the scale.*

3.2.5 Hydrogeochemical reactions in the absence of CO_2

Only a few reactions take place between the seal and the brine in the absence of CO_2 (Figure 3.8). Thus initially, a dissolution of chalcedony and siderite takes place while a small amount of hematite precipitates. For the rest of the experiment no significant reactions take place. Mass balance calculations indicate that 0.5% of the chalcedony and 0.2% of the siderite originally present in the seal samples dissolves during the experiment.

An overview of the mineralogical changes during the experiments with the seal mudstone samples is shown in Table 3.10. Even in the presence of CO_2, only insignificant changes in the mineralogical composition of the seal mudstone occur during the experiments.

Table 3.10 Overview of mineralogical changes in the experiments seal mudstones samples in the absence and presence of CO_2, based on mass balances of the model output.

		Absence of CO_2		Presence of CO_2	
	Composition start	Composition end	Fraction of mineral reacted	Composition end	Fraction of mineral reacted
	(vol%)	(vol%)	(%)	(vol%)	(%)
Quartz	13.6	13.6	n.i.	13.6	n.i.
Opal	1.0	1.0	0.02	1.0	0.2
Plagioclase	2.5	2.5	n.i.	2.5	n.i.
Siderite	3.9	3.9	0.0003	3.9	0.0004
Pyrite	1.1	1.1	n.i.	1.1	n.i.
Heulandite	11.4	11.4	0	11.4	0.14
Muscovite/Illite	37.7	37.7	n.i.	37.7	0.005
Smectite	28.7	28.7	n.i.	28.7	n.i.
Sum	100	100		100	

Additionally, calcite was found to dissolve in the model for the experiment with CO_2.

As for the reactions between reservoir and brine in the absence of CO_2 we expected no changes in the batch experiments as the experiments should start out as conditions that has equilibrated over millions of years. In the case of the Seal samples, we have no measurements of the actual pore fluid composition that these rocks are in equilibrium with. The P50 composition of the produced water from the reservoir is the best likely starting point but we also know that this composition is in equilibrium with a totally different mineral assemblage and that fluid flow and proximity to salt in the subsurface most likely has increased the TDS over time. In addition, we know that we by preparing grounded samples most likely inflicted broken surfaces and thus induced the reactivity. This is true mostly for coarser grained phases such as heulandite and opal whereas it likely has minor effect on the clay minerals. The preparation of the samples also exposed any mineral precipitates from the original pore fluids in the sample.

As for the reservoir rocks the end water composition from the experiments without CO_2 will serve as a good starting point in new experiments as this composition has had the chance to equilibrate with the rock and thus will limit the unnecessary mineral reactions.

3.2.6 Hydrogeochemical reactions in the presence of CO_2

As for the experiments with reservoir samples, the most prominent reaction between the seal and CO_2 is a substantial dissolution of calcite at the start of the experiment. This is followed

by a smaller continuous dissolution. Additionally, siderite and rhodochrosite dissolves, after which equilibrium is reached and the dissolution ceases. A continuous dissolution of illite takes place. The dissolution of illite is not detected by the petrographic analysis and therefore the nature of the Fe-containing mineral responsible for the observed increase in the Fe concentration is uncertain. The dissolution of this iron bearing mineral is very small (*c.* 0.05 ‰ of the illite is predicted to dissolve by the model, Table 3.10)). Such a small change may not be detected by the petrographic analysis.

The model predicts a continuous and not unimportant precipitation of heulandite. This contradicts with the petrographic analysis that indicate heulandite dissolution. The precipitation of heulandite is, however, important in regulating the aqueous concentration of not only the Si and Al but also Fe. The discrepancy between modelled and petrographic results may be due to uncertainties in the chemical composition of heulandite and more importantly the solubility. Additionally, the crushing of the sample material prior to the experiments may have exposed mineral surfaces that are otherwise not exposed and therefore not reactive. The geochemical model is calibrated against the experimentally observed changes in the brine composition resulting most from reactions with crushed samples while the petrographic analysis is made on an uncrushed piece of sample material.

In summary, the presence of CO_2 induces a number of reactions in the seal. Most important is an increase in the dissolution of calcite and siderite in the beginning of the experiment and dissolution of an Fe-bearing mineral.

4. Conclusions

The following major conclusions can be made from the batch experiments with either reservoir samples or seal rock mudstone in the absence and presence of CO_2:

- For the CO_2 and reservoir system, the results show that the presence of CO_2 leads to:
    - A significant increase in the initial dissolution of calcite followed by reprecipitation of calcite. Calcite reprecipitation is not identified in the absence of CO_2. Although significant calcite dissolution cannot be confirmed by the petrographic analysis, the dissolution of calcite during the experiments is crucial to fit the modelled concentrations of the components of the carbonate system (pH, alkalinity and Ca) to the measured values.
    - An increase in the dissolution of Mn-bearing siderite followed by precipitation of a "pure Fe" siderite. Reprecipitation of siderite does not take place in the absence of CO_2. Reprecipitation of siderite is not observed by the petrographic analysis. Alternatively, dissolution of a siderite with a different chemical composition or reprecipitation of ironhydroxides may explain the relatively lower release of Fe to solution compared to Mn.
    - Dissolution of an Fe-containing mineral. In the model berthierine has been applied.
    - Mass balance considerations of the CO_2 and reservoir system indicate that only small fractions of the reservoir rock react during the experiment. Thus, the composition of the sandstone after the experiments calculated by mass balance considerations of the results of the geochemical model equals that determined by point counting prior to the experiment.
    - The presence of hydrocarbons does not seem to affect the nature of the dissolution/precipitation processes between the Paleocene sandstone reservoir of the Nini West Field and CO_2. The presence of hydrocarbons may affect the reaction rates, which could be due to hydrocarbons blocking some of the reactive sites on the minerals.
- The geochemical model for the seal is less constraint since only a limited number of mineral reactions were identified by the petrographic analysis. The results for the seal are therefore associated with larger uncertainties. The results indicate that for the seal, the presence of CO_2 may lead to:
    - Increased dissolution of calcite and siderite
    - Dissolution of an Fe-bearing mineral. The identification of this mineral is uncertain. In the model illite was used.
    - It is unclear whether heulandite dissolves or precipitates in the presence of CO_2 since contradictory results are obtained by the petrographic analysis and the model.
    - Based on mass balances it is estimated only an insignificant fraction of the seal mudstone has reacted during the experiment. Thus, the composition of the seral mudstone after the experiments calculated by mass balance

considerations of the results of the geochemical model equals that determined by point counting prior to the experiment.

- The results of this study suggest that only the minor constituents of the reservoir and seal rock material is reactive towards CO_2.
- In both the reservoir and seal reactions associated with initial brine chemical composition and the rock matrix was observed suggesting that the starting brine composition estimated from produced water should be altered in future experiments. We suggest using the chemical composition measured at the end of the experiments without CO_2 as a starting point in new experiments.

5. Recommendations

Although much information is achieved from the results of the batch experiments, subsequent studies can help increase our knowledge of the hydrogeochemical reactions between CO_2, and the Paleocene sandstone reservoir of the Nini West Field and the overlying seal. Recommendations for further studies include:

- Investigation of the effect of impurities in the CO_2.
  The presence of impurities such as NO_x and SO_x in the injected CO_2 will give rise to additional acidification which generally increases dissolution rates of most host rock minerals. In addition, the impurities might cause oxidation/reduction of the Fe bearing clay of the glauconite, with unknown consequences for their stability. The "impure" gasses are all redox active and reaction rates are fairly fast, meaning that mainly the near-well environment would be affected. Therefore, the effect of impurities in the CO_2 on the hydrogeochemical reactions between reservoir and impure CO_2 should be investigated as suggested in Greensand phase 2.

- Further investigation of the seal reactivity towards CO_2.
  The obtained geochemical results for the reactivity of the seal towards CO_2 is afflicted with larger uncertainties due to the limited mineralogical changes observed by the petrographic analysis and unknowns with respect to thermodynamic properties of the clays and zeolite mineral. Therefore, further geochemical modelling with improved input parameters from the petrographic analysis is recommended as suggested in the proposed phase 2 of the Greensand project.

6. References

André, L., Audigane, P., Azaroual, M. and Menjoz, A. (2007) Numerical modeling of fluid–rock chemical interactions at the supercritical CO_2–liquid interface during CO_2 injection into a carbonate reservoir, the Dogger aquifer (Paris Basin, France). Energy Convers. Manage. 48, 1782-1797.

Appelo, C.A.J., and Postma, D. 2005. Geochemistry, Groundwater and Pollution. 2nd Edition. Published by A.A. Balkema Publishers, Leiden, The Netherlands, a member of Taylor and Francis pls. ISBN 04 1536 421 3

Blanc, P., Lassin, A., Piantone, P. Azaroual, M., Jacquemet, N., Fabbri, A., Gaucher, E.C. (2012)Thermoddem: A geochemical database focused on low temperature water/rock interactions and waste materials, Applied Geochemistry, 27(10), Pages 2107-2116, https://doi.org/10.1016/j.apgeochem.2012.06.002.

Cantucci, B., Montegrossi, G., Vaselli, O., Tassi, F., Quattrocchi, F. and Perkins, E.H. (2009) Geochemical modeling of CO_2 storage in deep reservoirs: The Weyburn Project (Canada) case study. Chem. Geol. 265, 181-197.

Chang, Yih-Bor, Coats, Brian K., Nolen, James S 1998. A Compositional Model for CO_2 Floods Including CO_2 Solubility in Water. SPE Reservoir Evaluation & Engineering, 1 (2), 55-160.

Hillier, S., 1999. Use of an air brush to spray dry samples for X-ray powder diffraction: Clay Minerals 34, 127-135.

Holmslykke, H.D., Weibel, R.,, Lorentzen, H.J., Schovsbo, N., 2021. Response of the Paleocene sandreservoir and seal of the Nini Field to CO_2 – results of batch experiments- Project Greensand phase 1 WP2. Geological Survey of Denmark and Greenland Report 2021/39.

Hörbrand T., Baumann, T., Moog, H. C. (2018). Validation of hydrogeochemical databases for problems in deep geothermal energy. Geothermal Energy. 6:20.

Olsen, D., Holmslykke, H.D., Weibel, R., Schovsbo, N., 2020. Setup and sample program of CO2 experiments. Greensand Phase 0. Danmarks og Grønlands geologiske undersøgelser, report 2020/19.

Palandri, J.L. and Kharaka, Y.K. (2004) A Compilation of Rate Parameters of Water-mineral Interaction Kinetics for Application to Geochemical Modeling. National Energy Technology Laboratory, U.S. Department of the Interior, U.S. Geological Survey.

Parkhurst, D.L. and Appelo, C.A.J. (2013) Description of input and examples for PHREEQC version 3 - A computer program for speciation, batch-reaction, one-dimensional transport, and inverse geochemical calculations, U.S. Geological Survey Techniques and Methods.

Ragnarsdottir K. (1993) Dissolution kinetics of heulandite at pH 2-12 and 25°C. Geochimica et Cosmochimica Acta, 57, 2439-2449.

Rowe, A.M., and Chou, J.C.S 1970. Pressure-volume-temperature-concentration relation of aqueous sodium chloride solutions. Journal of Chemical & Engineering Data 1970 15 (1), 61-66

Stookey L. L. (1970) Ferrozine—a new spectrophotometric reagent for iron. *Anal. Chem*. **42,** 779–781.

Stookey L. L., 1970. Ferrozine—a new spectrophotometric reagent for iron. Anal. Chem. 42, 779–781.

Weibel R., Keulen N., Olivarius M., Malkki, S.N., Holmslykke H.D., Mohammadkhani. S-. Olsen, D., Schovsbo N. (2021) Petrography and mineralogy of greensand in the Nini area including mineral reactions in CO_2 flooding experiments. Greensand Project Phase 1 WP2. Danmarks og Grønlands geologiske undersøgelser, report 2021/40.

Appendix 2

Results of BET analysis

Lab.no.	Sample no.	Sample ID	Depth (m, MD)	Formation	BET m^2/g
210201	NI4-1762.27	13	1762.27	Horda Fm	n.a.
210202	NI4-1748.65	15	1748.65	Horda Fm	30.5
210203	NI4-1748.65	15 EX	1748.65	Horda Fm	39.2
210204	NI4-1748.70	15C	1748.65	Horda Fm	n.a.
210205	NI4-1748.70 EX	15C EX	1748.70	Horda Fm	32.4
210206	NI4-1775.27C	92C	1775.27	Frigg sand	12.8
210207	NI4-1776.27C	95C	1776.27	Frigg sand	11.9
210208	NI4-1777.27C	98C	1777.27	Frigg sand	10.9
210209	NI4-1777.32	98	1777.32	Frigg sand	16.3
210210	NI4-1777.27	98B	1777.27	Frigg sand	2.22
210211	NI4-1779.19C	104C	1779.19	Frigg sand	12.1
210212	NI4-1779.32 EX	104 EX	1779.32	Frigg sand	16.9
210213	NI4-1779.19 EX	104B EX	1779.19	Frigg sand	2.90

Appendix 3

Chemical composition of the brine in the CO_2: brine : rock and the no CO_2 : brine : rock systems

Compositions not corrected for extracted volume during sampling or back-calculated to experimental conditions

Reservoir

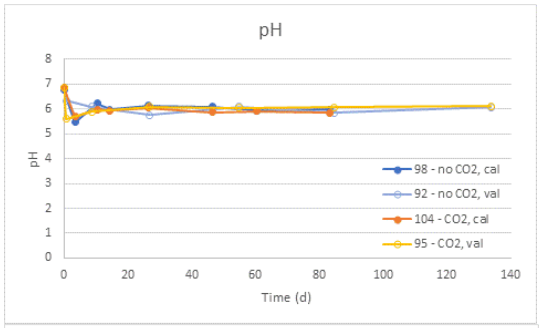

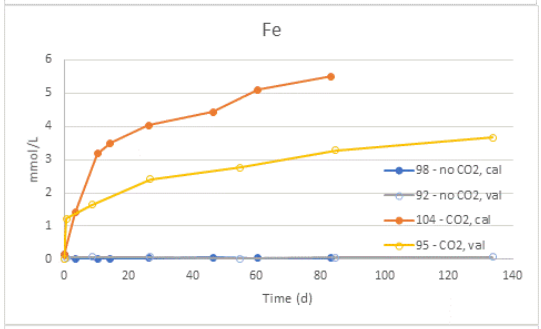

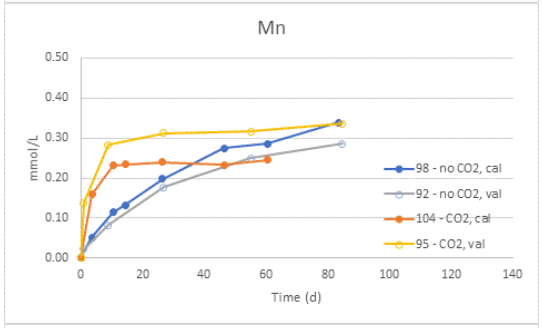

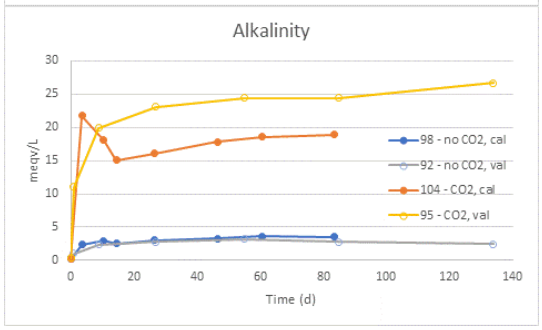

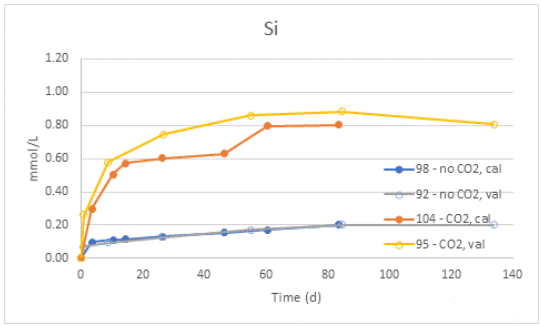

Reservoir HC

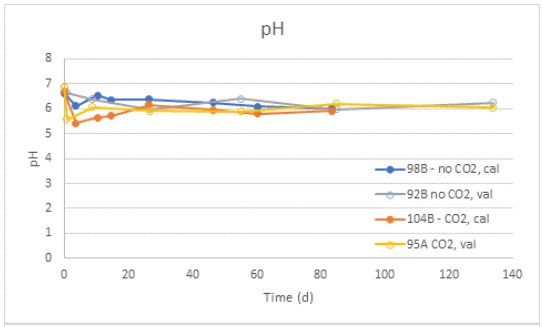

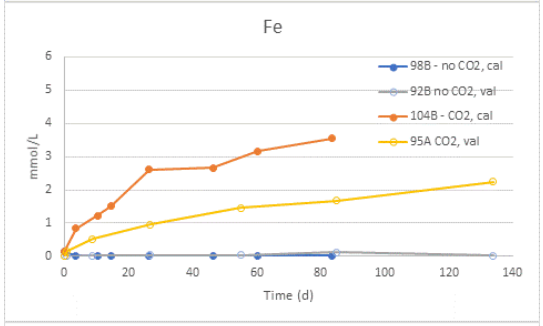

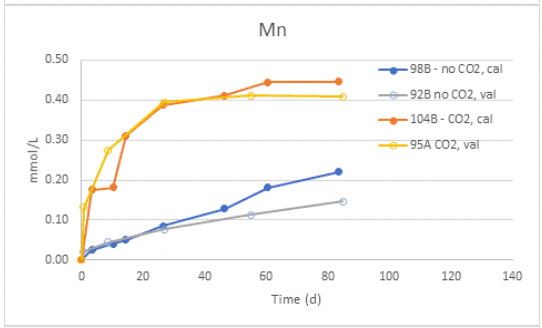

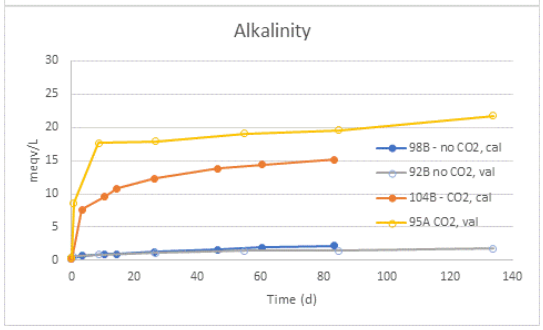

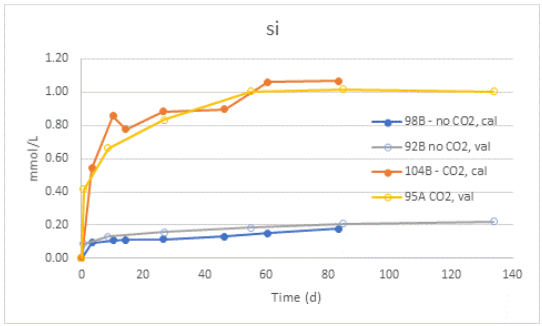

Seal

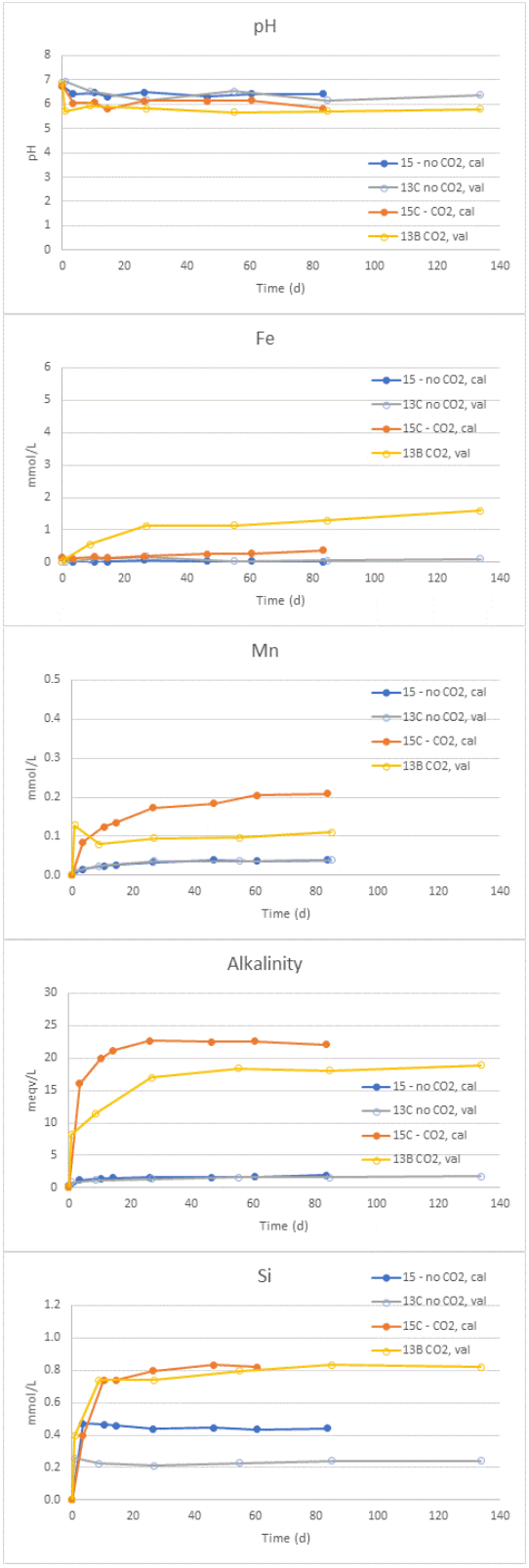
pH
pH
Time (d)
15 - no CO2, cal
13C no CO2, val
15C - CO2, cal
13B CO2, val
Fe
mmol/L
Time (d)
Mn
mmol/L
Time (d)
Alkalinity
meqv/L
Time (d)
Si
mmol/L
Time (d)

Appendix 4

Heavy metal release

Reservoir

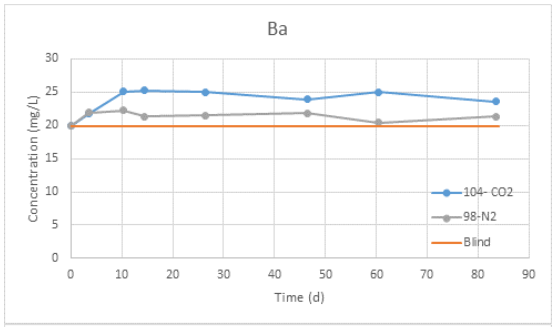

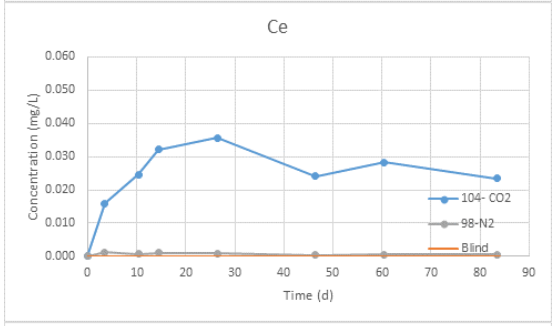

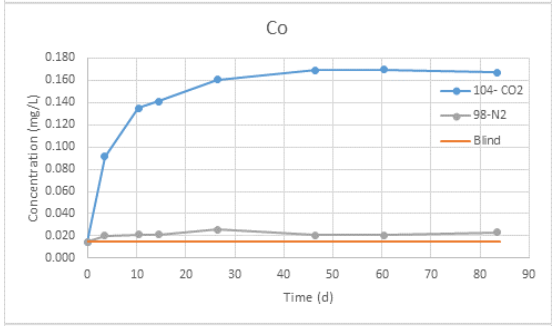

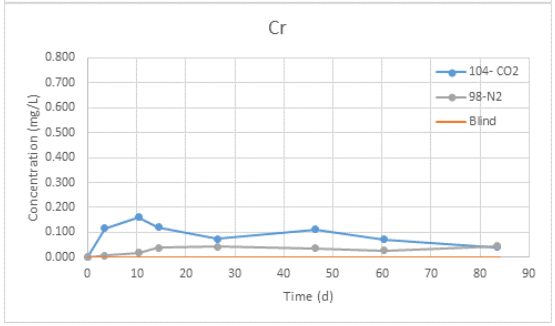

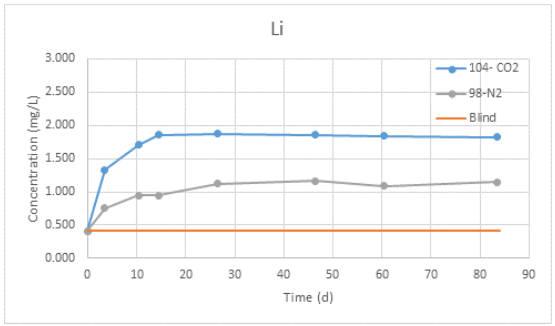

Reservoir HC

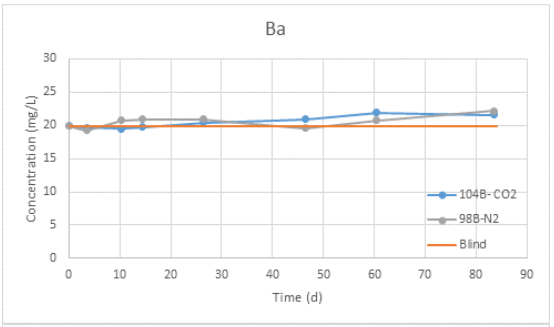

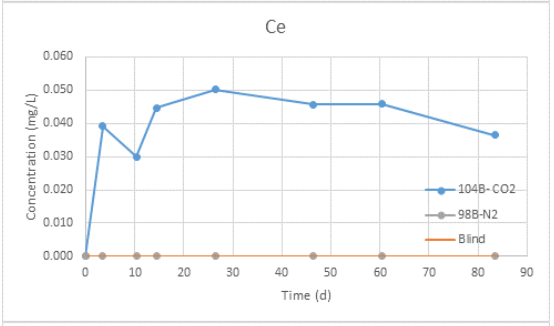

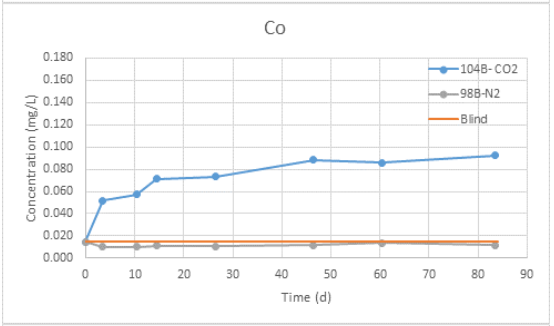

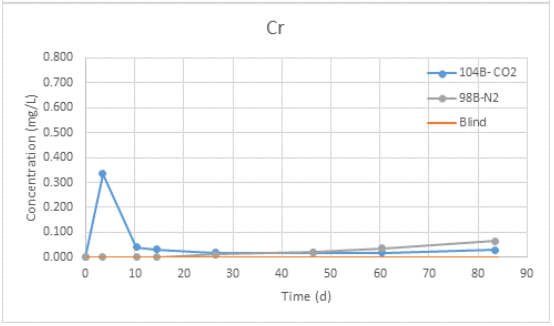

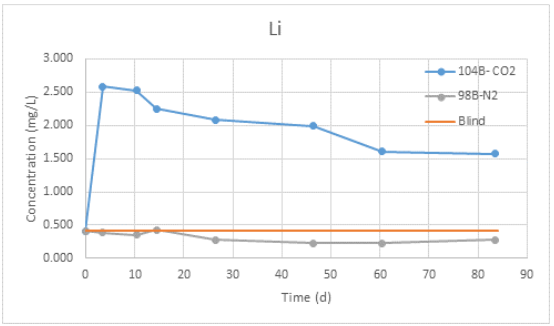

Reservoir

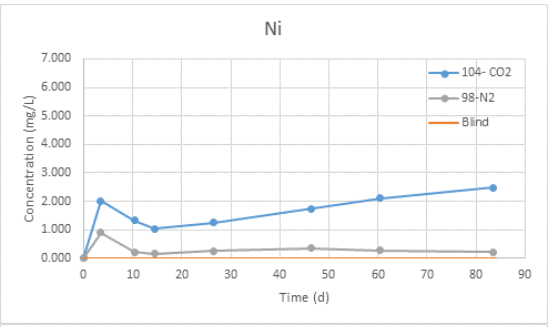

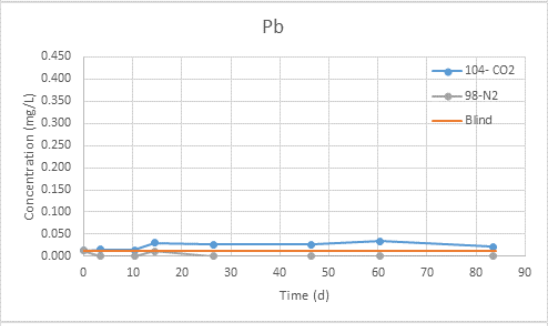

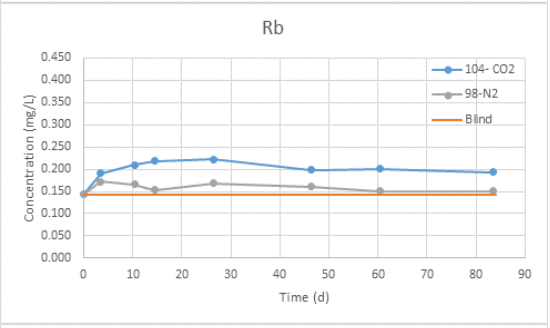

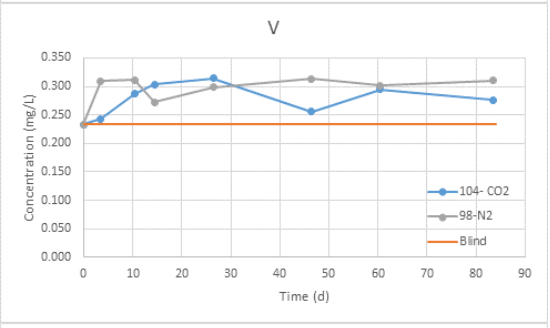

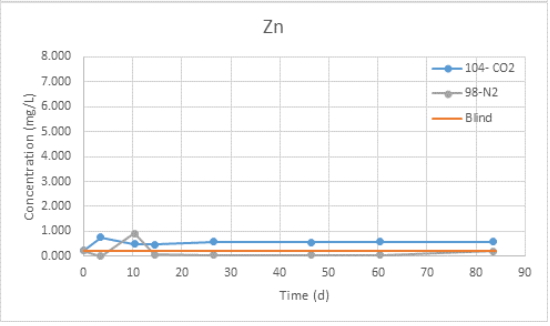

Reservoir HC

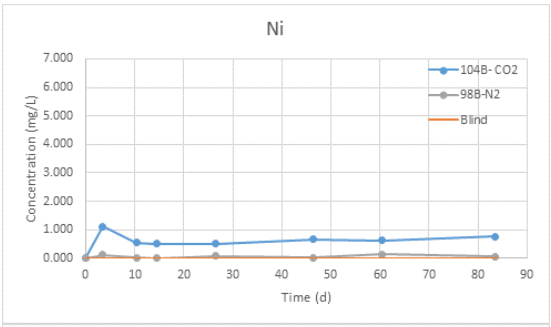

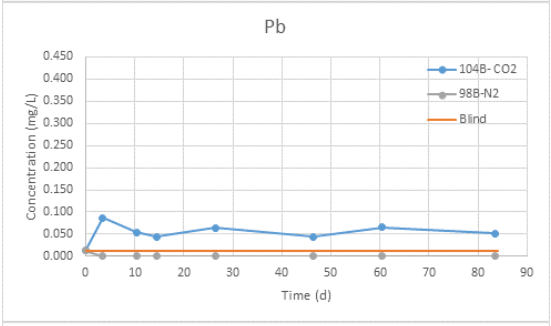

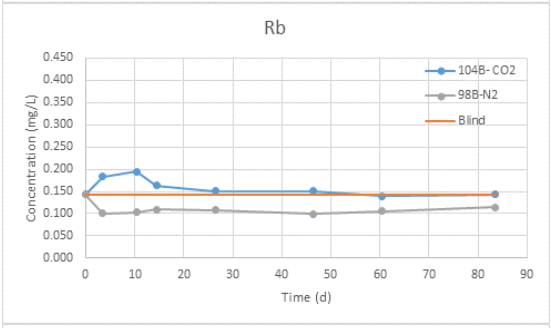

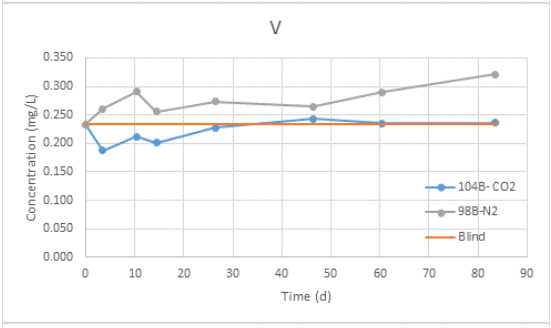

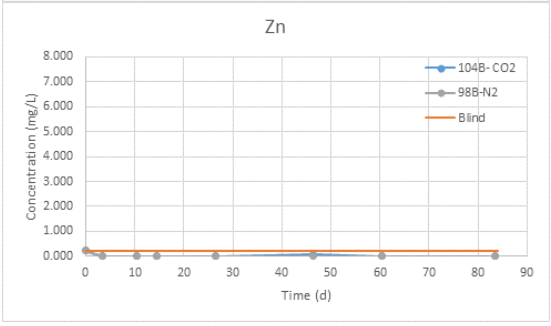

Seal

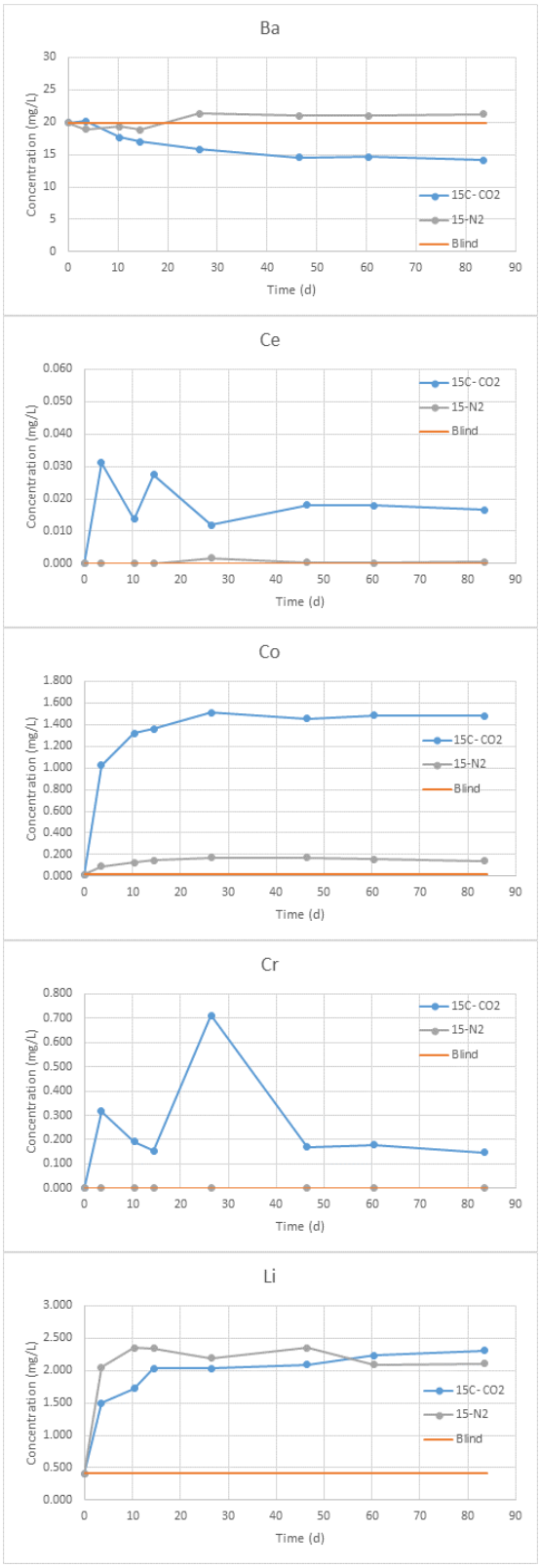
Ba
Concentration (mg/L)
Time (d)
15C- CO2
15-N2
Blind
Ce
Concentration (mg/L)
Time (d)
15C- CO2
15-N2
Blind
Co
Concentration (mg/L)
Time (d)
15C- CO2
15-N2
Blind
Cr
Concentration (mg/L)
Time (d)
15C- CO2
15-N2
Blind
Li
Concentration (mg/L)
Time (d)
15C- CO2
15-N2
Blind

Seal

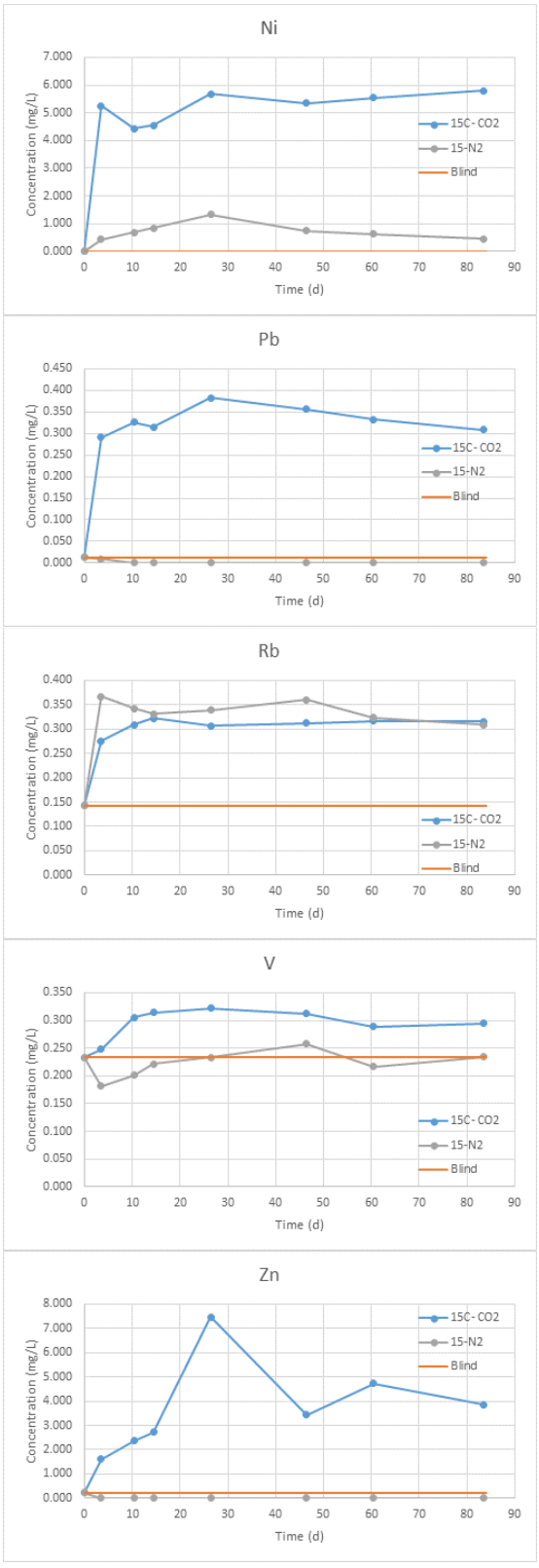
Ni
Concentration (mg/L)
Time (d)
15C- CO2
15-N2
Blind
Pb
Concentration (mg/L)
Time (d)
15C- CO2
15-N2
Blind
Rb
Concentration (mg/L)
Time (d)
15C- CO2
15-N2
Blind
V
Concentration (mg/L)
Time (d)
15C- CO2
15-N2
Blind
Zn
Concentration (mg/L)
Time (d)
15C- CO2
15-N2
Blind

Appendix 5

Kinetic parameters applied for the geochemical modelling

Reservoir, no CO_2

Kinetic parameters

			Acid mechanisms			Neutral mechanism		Alkali mechanism		
	SSA	m_0	log(k25)	E_a	n	log(k25)	E_a	log(k25)	E_a	n
	m^2/g	mol	($mol/m^2/s$)	(kJ/mol)	(-)	($mol/m^2/s$)	(kJ/mol)	($mol/m^2/s$)	(kJ/mol)	(-)
Almandine	1	0.3	-6.2	-5.2	1	-11.8	-10.7	-9.1	-8.7	-0.3
Smectite	4.5E-3	7	-10.98	23.6	0.34	-12.78	35.0	-16.52	58.9	-0.4
								Carbonate mechanism		
Siderite[b)]	2.9E-4	1.1	-3.19	36.1	0.500	-7.53	52.2	-5.11	34.8	0.500

[a)] Kinetic data for disordered dolomite, log(k) = -11.5
SSA: specific surface area

Equilibrium phases

Mineral	SI	m_0	Notes
Calcite	0	0.2	
$Al(OH)_3$	0		
Hematite	0		

Reservoir, CO_2

Kinetic parameters

			Acid mechanisms			Neutral mechanism		Alkali mechanism		
Mineral	SSA	m_0	log(k25)	E_a	n	log(k25)	E_a	log(k25)	E_a	n
	m^2/g	mol	($mol/m^2/s$)	(kJ/mol)	(-)	($mol/m^2/s$)	(kJ/mol)	($mol/m^2/s$)	(kJ/mol)	(-)
Almandine	5.30E-02	0.3	-6.2	-5.2	1	-11.8	-10.7	-9.1	-8.7	-0.3
Smectite	8.00E-05	7	-10.98	23.6	0.34	-12.78	35.0	-16.52	58.9	-0.4
Berthierine [a)]	10	0.2	-11.11	88.0	0.5	-12.52	88.0	-	-	-
								Carbonate mechanism		
Siderite_2[b)]	2.15E-06	1.1	-3.19	36.1	0.500	-7.53	52.2	-5.11	34.8	0.500

[a)] Kinetic data assumed equivalent to chlorite
[b)] Kinetic data for disordered dolomite

Equilibrium phases

Mineral	SI	m_0	Notes
Calcite	0	0.2	
Siderite	0	1.1	Dissolve only, log(k) = -10.63
$Al(OH)_3$	0		
Hematite	0		

Reservoir HC, no CO_2

Kinetic parameters

			Acid mechanisms			Neutral mechanism		Alkali mechanism		
	SSA	m_0	log(k25)	E_a	n	log(k25)	E_a	log(k25)	E_a	n
	m^2/g	mol	($mol/m^2/s$)	(kJ/mol)	(-)	($mol/m^2/s$)	(kJ/mol)	($mol/m^2/s$)	(kJ/mol)	(-)
Almandine	1	0.3	-6.2	-5.2	1	-11.8	-10.7	-9.1	-8.7	-0.3
Smectite	4.5E-3	7	-10.98	23.6	0.34	-12.78	35.0	-16.52	58.9	-0.4
								Carbonate mechanism		
Siderite[b)]	2.9E-4	1.1	-3.19	36.1	0.500	-7.53	52.2	-5.11	34.8	0.500

[a)] Kinetic data for disordered dolomite, log(k) = -11.5

Equilibrium phases

Mineral	SI	m_0	Notes
Calcite	0	0.2	
$Al(OH)_3$	0		
Hematite	0		

Reservoir HC, CO_2

Kinetic parameters

			Acid mechanisms			Neutral mechanism		Alkali mechanism		
Mineral	SSA	m_0	log(k25)	E_a	n	log(k25)	E_a	log(k25)	E_a	n
	m^2/g	mol	($mol/m^2/s$)	(kJ/mol)	(-)	($mol/m^2/s$)	(kJ/mol)	($mol/m^2/s$)	(kJ/mol)	(-)
Almandine	5.30E-02	0.3	-6.2	-5.2	1	-11.8	-10.7	-9.1	-8.7	-0.3
Smectite	2.00E-05	7	-10.98	23.6	0.34	-12.78	35.0	-16.52	58.9	-0.4
Berthierine [a)]	10	0.2	-11.11	88.0	0.5	-12.52	88.0	-	-	-
								Carbonate mechanism		
Siderite_2[b)]	4.15E-06	1.1	-3.19	36.1	0.500	-7.53	52.2	-5.11	34.8	0.500

[a)] Kinetic data assumed equivalent to chlorite
[b)] Kinetic data for disordered dolomite

Equilibrium phases

Mineral	SI	m_0	Notes
Calcite	0	0.2	
Siderite	0	1.1	Dissolve only, log(k) = -10.45
$Al(OH)_3$	0		
Hematite	0		

Seal, no CO_2

Kinetic parameters (from Ragnarsdottir 1993)

			Acid mechanisms			Neutral mechanism		Alkali mechanism		
	SSA	m_0	log(k25)	E_a	n	log(k25)	E_a	log(k25)	E_a	n
	m^2	mol	(mol/m^2/s)	(kJ/mol)	(-)	(mol/m^2/s)	(kJ/mol)	(mol/m^2/s)	(kJ/mol)	(-)
Heulandite	0.5	230.8				-15.75	74.5			

Equilibrium phases

Mineral	SI	m_0	Notes
Siderite	0	2.3E-4	
Chalcedony	0	2.4	
Hematite	0		

Seal, CO_2

Kinetic parameters

			Acid mechanisms			Neutral mechanism		Alkali mechanism		
Mineral	SSA	m_0	log(k25)	E_a	n	log(k25)	E_a	log(k25)	E_a	n
	m^2	mol	(mol/m^2/s)	(kJ/mol)	(-)	(mol/m^2/s)	(kJ/mol)	(mol/m^2/s)	(kJ/mol)	(-)
heulandite	0.5	500				-15.75	74.5			
Illite[a)]	400	13.7	-10.98	23.6	0.34	-12.78	35.0	-16.52	58.9	-0.40

[a)] Kinetic data assumed equivalent to smectite

Equilibrium phases

Mineral	SI	m_0	Notes
Calcite	0		
Siderite	0	2.5E-5	
Rhodochrosite	0	1.8E-4	
Chalcedony	0	2.4	Log(k) = -3.15
Hematite	0		

Appendix 6

Results of the geochemical modelling, uncleaned reservoir samples

Uncleaned reservoir samples in the absence of CO_2

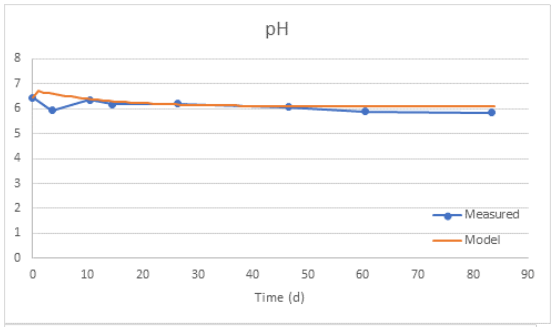

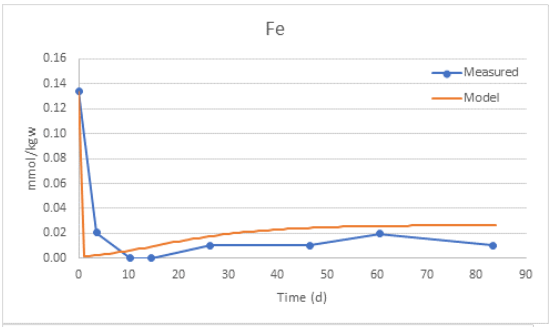

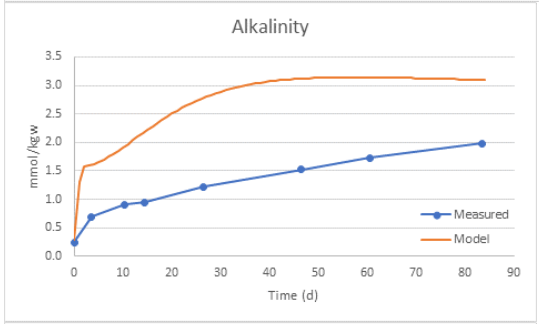

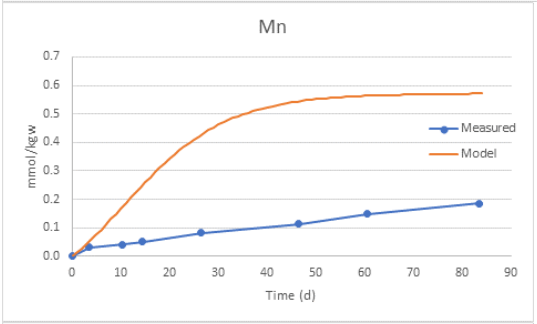

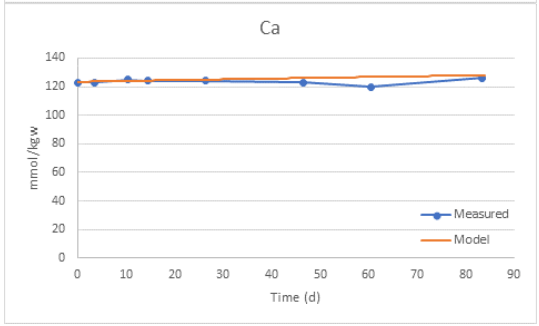

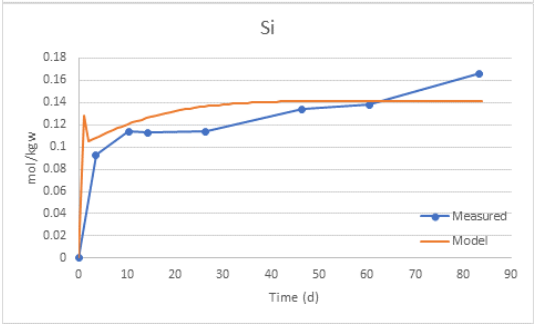

Uncleaned reservoir samples in the presence of CO_2